2017-01-01

Imaging Live Drosophila Brain With Two-Photon Fluorescence Microscopy

Syeed Ehsan Ahmed
University of Texas at El Paso, eshanahmed2012@gmail.com

IMAGING LIVE DROSOPHILA BRAIN WITH TWO-PHOTON FLUORESCENCE MICROSCOPY

SYEED EHSAN AHMED

Master's Program in Physics

APPROVED:

Chunqiang Li, Ph.D., Chair

Cristian E. Botez, Ph.D.

Chuan Xiao, Ph.D.

Charles Ambler, Ph.D.
Dean of the Graduate School

Dedication

Dedicated to my beloved family and friends. Thank you for believing in me and helping me throughout my journey.

IMAGING LIVE DROSOPHILA BRAIN WITH TWO-PHOTON FLUORESCENCE MICROSCOPY

by

SYEED EHSAN AHMED, B.Sc. in Physics

THESIS

Presented to the Faculty of the Graduate School of

The University of Texas at El Paso

in Partial Fulfillment

of the Requirements

for the Degree of

MASTER OF SCIENCE

Department of Physics

THE UNIVERSITY OF TEXAS AT EL PASO

August 2017

ACKNOWLEDGEMENTS

All praise and worthiness goes to Almighty Merciful Allah who has given me the opportunity, strength and ability to complete this work.

I would like to express my profound gratitude to my advisor, Dr. Chunqiang Li, for his mentorship, supervision and invaluable suggestions during my research. His continuous assessment and appropriate guidance enabled me to develop as a scientist and complete my research effectively.

I would like to thank Dr. Cristian Botez for his enthusiasm and perseverance as the chair of the department of Physics and for the kindness and guidance he has showed during our interactions.

I would also like to thank all my group members in the Biophotonics laboratory, especially Dr. Yu Ding for his constant support and guidance throughout my thesis work. I would like to take the opportunity to express my gratitude to all members of the faculty I have encountered from the Department of Physics at UTEP through their lectures, guidance and the support outside the classroom.

And lastly, my sincerest gratitude goes to my parents and my family for their continuous support in every situation towards the completion of my thesis.

ABSTRACT

Two-photon fluorescence microscopy is an imaging technique which delivers distinct benefits for *in vivo* cellular and molecular imaging. Cyclic adenosine monophosphate (cAMP), a second messenger molecule, is responsible for triggering many physiological changes in neural system. However, the mechanism by which this molecule regulates responses in neuron cells is not yet clearly understood. When cAMP binds to a target protein, it changes the structure of that protein. Therefore, studying this molecular structure change with fluorescence resonance energy transfer (FRET) imaging can shed light on the cAMP functioning mechanism. FRET is a non-radiative dipole-dipole coupling which is sensitive to small distance change in nanometer scale. In this study we have investigated the effect of dopamine in cAMP dynamics *in vivo*. In our study two-photon fluorescence microscope was used for imaging mushroom bodies inside live *Drosophila melanogaster* brain and we developed a method for studying the change in cyclic AMP level.

TABLE OF CONTENTS

LIST OF TABLES

LIST OF FIGURES

CHAPTER 1: TWO-PHOTON MICROSCOPY

1.1 INTRODUCTION

In the last two decades several laser-scanning microscopy techniques have been developed centered on the non-linear optical phenomena and that led to a variety of powerful imaging tools. Two-Photon Microscopy, Coherent anti-Stokes Raman Scattering and Second Harmonic Generation Microscopy are among those imaging tools and has an intense impact in the field of biological imaging due to their novel techniques over conventional microscopy. Two-photon microscopy is the current chosen technique for live cell imaging for extended time period and to image deep within the tissues due to its noninvasive investigation in three dimension with sub-micrometer resolution, increased penetration depth and efficient light detection. Two photon excitation of fluorophores results from the simultaneous absorption of two photon [1]

Two-photon microscopy is a non-linear optical process for fluorescence imaging technique in which fluorescent molecules are stimulated by the simultaneous absorption two photons. In two-photon microscopy fluorescent tag within a sample is excited by a laser and the emitted light is measured by detectors. Unlike the single-photon excitation, the lasers used in two-photon microscopy excite by using two long wavelength photons which are less damaging and can penetrate deep within the tissues. In addition the excitation is only achieved near the focal plane where the laser light is most intense due to the near simultaneous absorption of two photons. The focused excitation results sharper image and little tissue damage to the regions above and below the focal plane.

1.2 HISTORY OF TWO-PHOTON MICROSCOPY

In 1873 a theoretical analysis done by Ernst Abbe suggested that diffraction of the illuminating light limits the optical microscopic resolution [2]. This study led people like August Köhler to develop the first ultraviolet absorption microscope in 1904. During his study Köhler observed that the barium platinum cyanide crystal fluorescing in the visible spectrum indicating a longer wavelength than the ultraviolet light [3]. This study motivated scientists to develop the first fluorescence microscope.

In 1931 Maria Göppert-Mayer first described the concept of multiphoton excitation in her doctoral dissertation based on the hypothesis of two-photon quantum transition in particle [4]. After the invention of laser in 1960, In 1961 Peter Franken who is consider as the father of non-linear optics along with his group focused a high powered ruby laser onto a quartz crystal to demonstrate the second harmonic generation of light [5]. They demonstrated that the ruby laser light with wavelength λ, propagating through quartz will produce light of wavelength $\lambda/2$ due to the process of second harmonic generation. Then, in 1963, W. Kaiser and Charles Geoffrey Blythe Garrett demonstrated their observation of two-photon excitation (TPE) in a $CaF_2:Eu^{2+}$ crystal and first to publish results of TPE [6]. They also found out that the fluorescence of natural colors can also be excited by TPE. Since then nonlinear optics moved from a laboratory curiosity to a tool important for spectroscopy, metrology and biomedical applications. After almost three decades the Göppert-Mayer's hypothesis was at last affirmed. Three-photon excitation spectroscopy has likewise been depicted by the correlation with the two-photon forms [7].

1.3 THEORY OF TWO-PHOTON ABSORPTION

In single photon absorption and two photon absorption the results in a blue and red shift from the incident light to the emitted light. In case of single photon absorption the reason behind the result is due to the energy of the incident excitation light is equal to the energy gap between a fluorescent molecule ground state and an excited vibronic state,

$$E_p = \Delta E_s = \frac{hc}{\lambda}. \tag{1.1}$$

The molecule undergoes a non-radiative transition to a lower vibronic state before decaying back to the ground state with the emission of fluorescent light. This interaction is depicted in Figure (1.1).

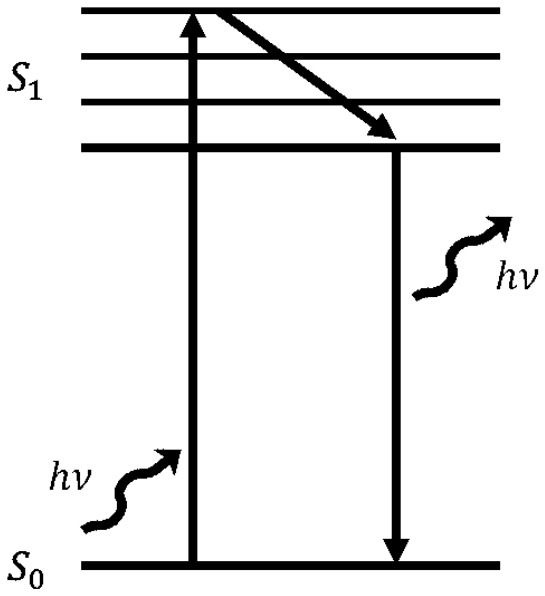

Figure 1.1 - One-Photon Excitation.

In case of two-photon absorption, two distinct photons excite a fluorescent molecule to an excited vibronic state. Here, energy of the incident excitation light is half the energy gap between a fluorescent molecule ground state and an excited vibronic state,

$$E_p = \frac{1}{2}\Delta E_s = \frac{hc}{2\lambda}. \tag{1.2}$$

The molecule undergoes the same type of non-radiative decay like single photon after it's been excited with two photons. This interaction is depicted in Figure (1.2).

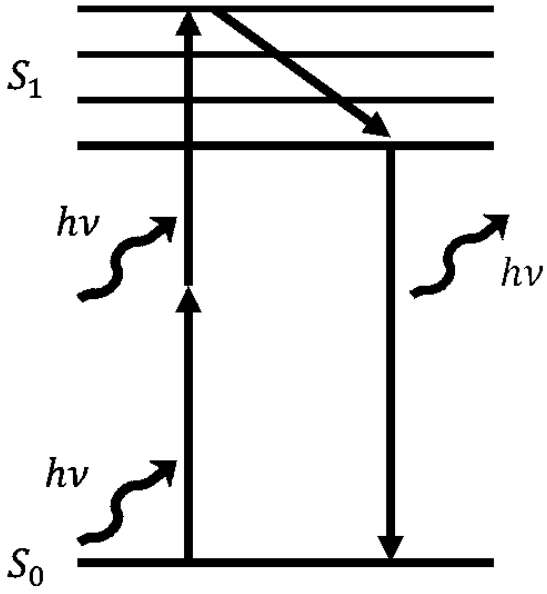

Figure 1.2 - Two-Photon Excitation.

Perturbation theory is a powerful tool to model the interaction between light and atom when the interaction is not strong. According to the approach, the Hamiltonian can be expressed as,

$$\widehat{H} = \widehat{H_0} + \hat{V}(t). \tag{1.3}$$

Where $\widehat{H_0}$ is the unperturbed time independent Hamiltonian and the time dependent interaction energy is $\hat{V}(t)$.

The time dependent interaction energy can be written as

$$\hat{V}(t) = -\hat{\mu}\tilde{E}(t), \tag{1.4}$$

Here the dipole moment of the molecule is expressed as $\hat{\mu} = -e\hat{r}$. The field is considered a monochromatic wave of the form

$$\tilde{E}(t) = Ee^{-i\omega t} + E^{*}e^{i\omega t}. \tag{1.5}$$

Assuming the energy eigenstates of the unperturbed system $u_n(\vec{r})$ are known and they satisfy the eigenvalue equation. Therefore the associated wave function may be represented by,

$$\psi_n(\vec{r}, t) = u_n(\vec{r})e^{-i\omega_n t}, \tag{1.6}$$

Here, $\omega_n = \frac{E_n}{\hbar}$.

Also the eigenvalue equation

$$\widehat{H_0}u_n(\vec{r}) = E_n u_n(\vec{r}) \tag{1.7}$$

The problem appears to solve the time-dependent Schrödinger equation with the time-dependent interaction potential $\hat{V}(t)$

$$i\hbar\frac{\partial\psi(\vec{r},t)}{\partial t} = \left(\widehat{H_0} + \hat{V}(t)\right)\psi(\vec{r},t). \tag{1.8}$$

Given that they form a complete set, the complete solution can be expressed as a linear combination of the eigenstates with time dependent probability densities $a_k(t)$

$$\psi(\vec{r},t) = \sum_k a_k(t)u_k(\vec{r})\, e^{-iw_k t}, \tag{1.9}$$

Substituting this solution into the time-dependent Schrodinger equation Eq. (1.8),

$$i\hbar\sum_k \frac{da_k}{dt}u_k(\vec{r})e^{-i\omega_k t} + i\hbar\sum_k a_k(t)(-i\omega_k)u_k(\vec{r})e^{-i\omega_k t}$$
$$= \sum_k a_k(t)E_k u_k(\vec{r})e^{-i\omega_k t} + \sum_k a_k(t)\hat{V}u_k(\vec{r})e^{-i\omega_k t}.$$

Using $E_k = \hbar\omega_k$, this expression can be simplified as

$$i\hbar\sum_k \frac{da_k}{dt}u_k(\vec{r})e^{-i\omega_n t} + \sum_{\cancel{k}} \cancel{a_k(t)E_k u_k(\vec{r})e^{-i\omega_k t}}$$
$$= \sum_{\cancel{k}} \cancel{a_k(t)E_k u_k(\vec{r})e^{-i\omega_k t}} + \sum_k a_k(t)\hat{V}u_k(\vec{r})e^{-i\omega_k t}. \tag{1.10}$$

This can be written as

$$i\hbar \sum_k \frac{da_k}{dt} u_k(\vec{r}) e^{-i\omega_n t} = \sum_k a_k(t) \hat{V} u_k(\vec{r}) e^{-i\omega_k t}$$

Using the orthonormality condition of eigenstates $u_k(\vec{r})$, the problem can be further simplified to

$$\int u_m^*(\vec{r}) u_k(\vec{r}) d^3r = \delta_{mk}$$

$$i\hbar \sum_k \frac{da_k}{dt} \left[\int u_m^*(\vec{r})\, u_k(\vec{r}) d^3r \right] e^{-i\omega_k t} = \sum_k a_k(t) \left[\int u_m^*(\vec{r}) \hat{V} u_k(\vec{r}) d^3r \right] e^{-i\omega_k t}$$

$$i\hbar \frac{da_m}{dt} = \sum_k a_k(t)\, V_{mk} e^{-i(\omega_k - \omega_m)t}$$

$$\frac{da_m}{dt} = \frac{1}{i\hbar} \sum_k a_k(t)\, V_{mk} e^{i\omega_{mk} t} \tag{1.11}$$

where $V_{mk} = \int u_m^*(\vec{r}) \hat{V} u_k(\vec{r}) d^3r$ are the matrix elements of the interaction potential $\hat{V}(t)$ and $\omega_{mk} = \omega_m - \omega_k$.

To solve the Eq. (1.11) we have to consider perturbation techniques. The probability densities $a_m(t)$ can be expanded in powers of an expansion parameter and the exponents represent the perturbation order which is the accepted number of photons. Let us consider λ as an expansion parameter. Then,

$$a_m(t) = a_m{}^{(0)}(t) + \lambda a_m{}^{(1)}(t) + \lambda^2 a_m{}^{(2)}(t) + \cdots, \tag{1.12}$$

Here, $N = 2$ corresponds to two-photon absorption therefore $a_k{}^{(2)}(t)$ will be of most important.

Replacing V_{mk} with λV_{mk}, and substituting (1.12) into (1.11) yields

$$\begin{aligned} &\frac{da_m{}^{(0)}(t)}{dt} + \lambda \frac{da_m{}^{(1)}(t)}{dt} + \lambda^2 \frac{da_m{}^{(2)}(t)}{dt} + \cdots \\ &\qquad = \frac{1}{ih}\sum_k \left(a_k{}^{(0)}(t) + \lambda a_k{}^{(1)}(t) + \lambda^2 a_k{}^{(2)}(t) + \cdots\right)\lambda V_{mk} e^{i\omega_{mk}t}, \end{aligned} \tag{1.13}$$

And for the Nth term,

$$\frac{da_m{}^{(N)}(t)}{dt} = \frac{1}{ih}\sum_k a_k{}^{(N-1)}(t) V_{mk} e^{i\omega_{mk}t}. \tag{1.14}$$

Assuming that in the absence of an applied field, the atom is in the ground state

$$a_g{}^{(0)}(t) = 1, \qquad a_k{}^{(0)}(t) = 0 \quad for \quad k \neq g,$$

It follows that for N = 1

$$\frac{da_k{}^{(1)}(t)}{dt} = \frac{1}{ih} a_g{}^{(0)}(t) V_{mg} e^{i\omega_{mg}t} = \frac{1}{ih} V_{mg} e^{i\omega_{mg}t}. \tag{1.15}$$

Now, V_{mg} can be represented as

$$V_{mg} = -\mu_{mg}\left(Ee^{-i\omega t} + E^{*}e^{i\omega t}\right), \tag{1.16}$$

Then Eq. (1.15) becomes,

$$\frac{da_m{}^{(1)}(t)}{dt} = \frac{-\mu_{mg}}{ih}\left(Ee^{-i\omega t} + E^{*}e^{i\omega t}\right)e^{i\omega_{mg}t}$$

$$\frac{da_m{}^{(1)}(t)}{dt} = \frac{-\mu_{mg}}{ih}\left(Ee^{i(\omega_{mg}-\omega)t} + E^{*}e^{i(\omega_{mg}+\omega)t}\right),$$

Integrating, we are able to get the representation of a one-photon absorption process,

$$a_m{}^{(1)}(t) = \frac{-\mu_{mg}}{ih}\int_0^t \left(Ee^{i(\omega_{mg}-\omega)t} + E^{*}e^{i(\omega_{mg}+\omega)t}\right)dt.$$

$$a_m{}^{(1)}(t) = \frac{\mu_{mg}E}{\hbar\left(\omega_{mg}-\omega\right)}\left[e^{i(\omega_{mg}-\omega)t} - 1\right] + \frac{\mu_{mg}E^{*}}{\hbar\left(\omega_{mg}+\omega\right)}\left[e^{i(\omega_{mg}+\omega)t} - 1\right]. \tag{1.17}$$

It can be estimated through restricting the driving frequency ω to be very close to the transition frequency ω_{mg}, then only the first term dominates and we have

$$a_m{}^{(1)}(t) \cong \frac{\mu_{mg}E}{\hbar\left(\omega_{mg}-\omega\right)}\left[e^{i(\omega_{mg}-\omega)t} - 1\right]. \tag{1.18}$$

Setting $N = 2$ we are able to get the two-photon absorption term,

$$\frac{da_n{}^{(2)}(t)}{dt} = \frac{1}{ih}\sum_m a_m{}^{(1)}(t)V_{nm}e^{i\omega_{nm}t}. \tag{1.19}$$

Substituting both Eqs. (1.18) and (1.16) into Eq. (1.19),

$$\frac{da_n{}^{(2)}(t)}{dt} = \frac{-1}{ih}\sum_m \{\frac{\mu_{mg}E}{\hbar(\omega_{mg}-\omega)}\left[e^{i(\omega_{mg}-\omega)t}-1\right]\}\left(Ee^{-i\omega t} + E^*e^{i\omega t}\right)\mu_{nm}Ee^{i\omega_{nm}t}, \tag{1.20}$$

We can omit the E^* term since we have considered the driving frequency to be very close to the transition frequency,

$$\frac{da_n{}^{(2)}(t)}{dt} = \frac{-1}{ih}\sum_m \frac{\mu_{mg}\mu_{nm}E}{\hbar(\omega_{mg}-\omega)}\left[e^{i(\omega_{mg}-\omega)t}-1\right]Ee^{i(\omega_{nm}-\omega)t}$$

$$\frac{da_n{}^{(2)}(t)}{dt} = \frac{-1}{ih^2}\sum_m \frac{E^2\mu_{mg}\mu_{nm}}{(\omega_{mg}-\omega)}\left[e^{i(\omega_{mg}+\omega_{nm}-2\omega)t}-e^{i(\omega_{nm}-\omega)t}\right]$$

$$\frac{da_n{}^{(2)}(t)}{dt} = \frac{-1}{ih^2}\sum_m \frac{E^2\mu_{mg}\mu_{nm}}{(\omega_{mg}-\omega)}\left[e^{i(\omega_{ng}-2\omega)t}-e^{i(\omega_{nm}-\omega)t}\right]. \tag{1.21}$$

In Eq. (1.22) only the first exponent term represent two-photon absorption therefore we may dropped the second exponent term,

$$\frac{da_n{}^{(2)}(t)}{dt} = \frac{-1}{ih^2}\sum_m \frac{E^2\mu_{mg}\mu_{nm}}{(\omega_{mg}-\omega)} e^{i(\omega_{ng}-2\omega)t}.$$

Now by integrating,

$$a_n{}^{(2)}(t) = -\frac{1}{i\hbar^2}\sum_m \frac{E^2\mu_{mg}\mu_{nm}}{(\omega_{mg}-\omega)}\int_0^t e^{i(\omega_{ng}-2\omega)t}dt$$

$$a_n{}^{(2)}(t) = \frac{1}{\hbar^2}\sum_m \frac{E^2\mu_{mg}\mu_{nm}}{(\omega_{mg}-\omega)}\left[\frac{e^{i(\omega_{ng}-2\omega)t}-1}{(\omega_{ng}-2\omega)}\right] \tag{1.22}$$

Here $a_n{}^{(2)}(t)$ is called the probability amplitude for two-photon absorption. Let us consider $p_n(t)^{(2)}$ is the probability for an atom in n state and time t. We know that the probability of two-photon absorption is the square of the probability amplitude $a_n{}^{(2)}(t)$,

$$p_n{}^{(2)}(t) = \left|a_n(t)^{(2)}\right|^2 = \left|\frac{1}{\hbar^2}\sum_m \frac{E^2\mu_{mg}\mu_{nm}}{(\omega_{mg}-\omega)}\right|^2 \left|\frac{e^{i(\omega_{ng}-2\omega)t}-1}{(\omega_{ng}-2\omega)}\right|^2. \tag{1.23}$$

Using the Euler's formula, we can further simplified the numerator in the second term,

$$\left|e^{i(\omega_{ng}-2\omega)t}-1\right|^2 = \left|\cos(\omega_{ng}-2\omega)t + i\sin(\omega_{ng}-2\omega)t - 1\right|^2$$

$$= \left[\cos(\omega_{ng}-2\omega)t + i\sin(\omega_{ng}-2\omega)t - 1\right]\left[\cos(\omega_{ng}-2\omega)t - i\sin(\omega_{ng}-2\omega)t - 1\right]$$

$$= 1 + \cos^2(\omega_{ng}-2\omega)t + \sin^2(\omega_{ng}-2\omega)t - 2\cos(\omega_{ng}-2\omega)t$$

$$= 2 - 2\cos(\omega_{ng} - 2\omega)t = 2[1 - \cos(\omega_{ng} - 2\omega)t]$$

Therefore putting this back to Eq. (1.23) we get,

$$\left|e^{i(\omega_{ng}-2\omega)t} - 1\right|^2 = 4\sin^2\frac{(\omega_{ng} - 2\omega)t}{2}, \tag{1.24}$$

Now from Eq. (1.23),

$$p_n{}^{(2)}(t) = \left|\frac{1}{\hbar^2}\sum_m \frac{E^2\mu_{mg}\mu_{nm}}{(\omega_{mg} - \omega)}\right|^2 \frac{4\sin^2\frac{(\omega_{ng} - 2\omega)t}{2}}{(\omega_{ng} - 2\omega)^2}. \tag{1.25}$$

Separating the time dependent and independent term we get,

$$p_n{}^{(2)}(t) = \left|\frac{E^2}{\hbar^2}\sum_m \frac{\mu_{mg}\mu_{nm}}{(\omega_{mg} - \omega)}\right|^2 \rho(\omega_{ng}, \omega, t), \tag{1.26}$$

where

$$\rho(\omega_{ng}, \omega, t) = \frac{4\sin^2\frac{(\omega_{ng} - 2\omega)t}{2}}{(\omega_{ng} - 2\omega)^2}, \tag{1.27}$$

Eq. (1.27) is plotted in Fig. (1.3). The function $\rho(\omega_{ng}, \omega, t)$ can be considered zero if we take in account the fact that the driving frequency is almost equal to the transition one ($\omega_{ng} \approx 2\omega$).

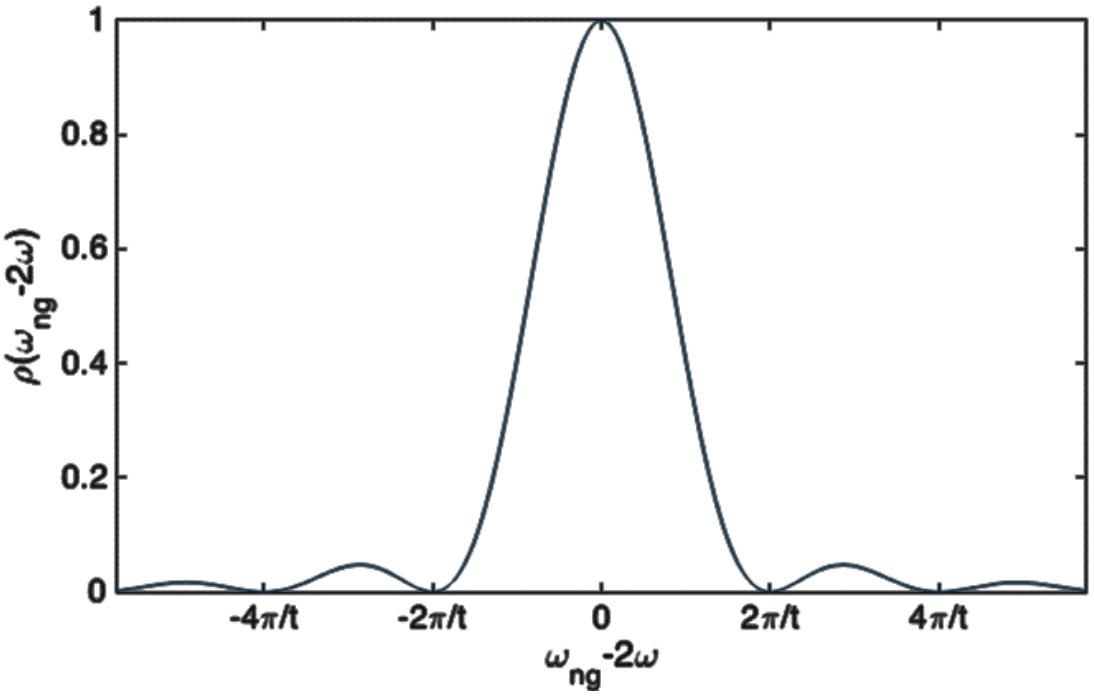

Fig. 1.3 - Probability density distribution of Eq. (1.27).

The value of $\rho(\omega_{ng}, \omega, t)$ can be approximated by using the L'Hopitals rule within the limit $2\omega \to \omega_{ng}$ and considering $\omega_{ng} = 2\omega$ when the peak value occurs,

$$\lim_{2\omega \to \omega_{ng}} \rho(\omega_{ng}, \omega, t) = \lim_{2\omega \to \omega_{ng}} \frac{4 \sin^2 \frac{(\omega_{ng} - 2\omega)t}{2}}{(\omega_{ng} - 2\omega)^2} = t^2.$$

The area under the curve in Fig. 1.2 must be constant since $\rho(\omega_{ng}, \omega, t)$ is a time-dependent probability density, this area can be approximated by

$$A = \frac{1}{2}\frac{4\pi}{t}t^2 = 2\pi t.$$

For $t \to \infty$ the function $\rho(\omega_{ng}, \omega, t)$ corresponds to an area of narrow peaked region which can be approximated by the Dirac delta function as

$$\lim_{t\to\infty} \rho\big(\omega_{ng}, \omega, t\big) = 2\pi t\delta\big(\omega_{ng} - 2\omega\big), \tag{1.28}$$

Substituting this into Eq. (1.26), gives

$$p_n{}^{(2)}(t) = \left|\frac{1}{\hbar^2}\sum_m \frac{E^2\mu_{mg}\mu_{nm}}{\big(\omega_{mg} - \omega\big)}\right|^2 2\pi t\delta\big(\omega_{ng} - 2\omega\big). \tag{1.29}$$

The local intensity cab be written as,

$$I = \frac{cn\varepsilon_0}{2}|E|^2. \tag{1.30}$$

Eq. (1.29) can be further simplified if we consider a parameter $\sigma_{ng}(\omega)$ which is known as the two-photon cross section and use the information from Eq. (1.30)

$$\sigma_{ng}(\omega) = \frac{4}{(cn\varepsilon_0)^2}\left|\frac{1}{\hbar^2}\sum_m \frac{\mu_{mg}\mu_{nm}}{\big(\omega_{mg} - \omega\big)}\right|^2 2\pi\delta\big(\omega_{ng} - 2\omega\big) \tag{1.31}$$

Now using the information in Eq. (1.30) along with the two-photon cross section we have

$$p_n{}^{(2)}(t) = \sigma_{ng}(\omega)I^2 t \tag{1.32}$$

Eq. (1.32) clearly depicts the important relation between the probability density of two-photon absorption and excitation intensity

$$p_n{}^{(2)} \propto I^2. \tag{1.33}$$

1.4 EXPERIMENTAL SETUP OF TWO-PHOTON FLUORESCENCE MICROSCOPE

1.4.1 LIGHT SOURCE

The two-photon microscope developed in our lab uses a femtosecond titanium-sapphire (Ti:Sapphire) laser source. The structure delivers pulses with a repetition frequency of 80 MHz and duration on the order of 100 fs. The pulsing light source limit the exposure of the sample and plays an important role to reduce damage caused to the sample by reducing the delivered average power. The framework can deliver peak powers more than 300 kW and the average power ranging from 0.5 W to 2.5 W. The wavelength is tunable and has a broad tuning range from 690nm to 1040nm which allows to excite wide variety of fluorophores. In two-photon absorption the excitation wavelength approximated as double the excitation wavelength of a single-photon excitation wavelength typically from 700nm to 1400nm. The most utilized fluorophores and dyes has single-photon excitation wavelength in the range from 350nm to 690nm therefore with our source we are transported to the near infrared region of the spectrum. The structure we are using provide prominent infiltration depth in case of biological specimens due to low absorption and dispersing which is caused by minimized absorption coefficients of the sample in the near infrared region.

1.4.2 WAVEPLATE AND POLARIZER

The light coming out of our light source is linearly polarized in the horizontal direction. There is a half waveplate attached to a rotary mounting right after the source which allows us to shift the polarization direction by rotating the slow and fast axes of the waveplate. A waveplate is characterized by its phase shift and a typical half waveplate introduces a phase shift of $\Gamma = \pi$ for a given thickness, birefringence and wavelength. A linearly polarized light with phase shift of π yields a rotation of 2θ where θ is the angle formed between the polarization vector and fast axis of the waveplate.

Following the half waveplate, the light passes through a polarizer made of birefringent material which splits the light by changing the polarization. The split lights with different linear polarization then filtered by taking account a light of certain polarization and the rest is reflected perpendicular to the path of the initial light. The femtosecond laser used in our laboratory does not require high intensity light and using the combination of waveplate and polarizer we can control the average power of the light. We obtain our desired power of the light by rotating the waveplate while keeping the polarizer fixed in a position. The intensity of a light while passing through a polarizer can be described by,

$$I = I_0 \cos^2 \beta, \tag{1.34}$$

This is known as the Malu's law where, I_0 and β are the intensities before and after the polarizer and the angle between the polarization vector and the axis of the polarizer respectively. In case of $\beta = 90°$ the whole light is blocked and the full intensity is transmitted when $\beta = 0°$.

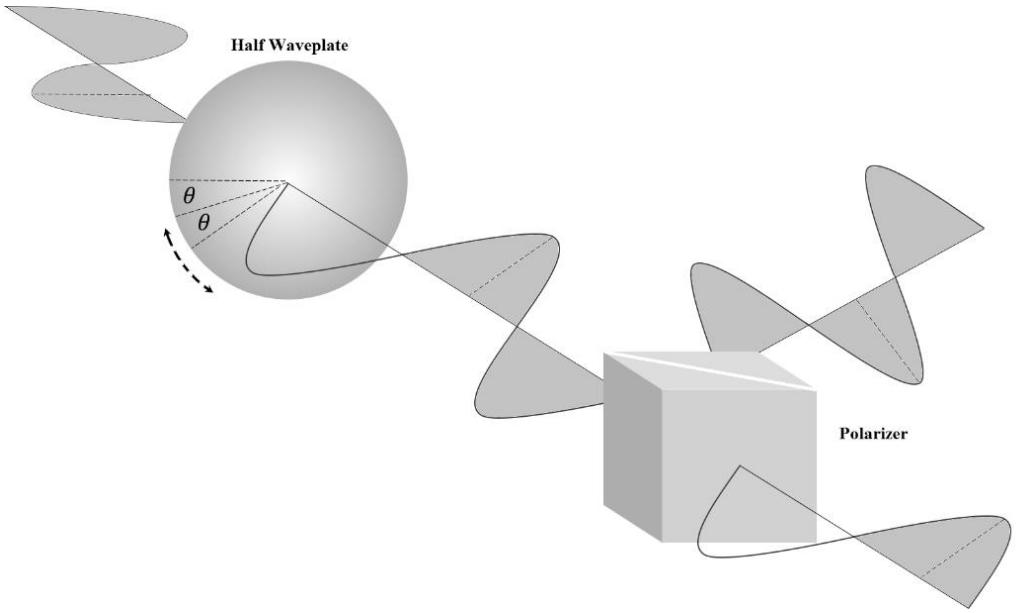

Figure 1.4 - Diagram of Intensity controlling system.

1.4.3 SCANNING PLATFORM

The scanning mechanism in our two-photon microscope is an essential component which allows us to produce images of dynamic cellular processes using a raster scanning method. With the scanning mechanism it is possible to image 320μm by 320μm images with 30 frames per second. The scanning platform contains a turning polygonal mirror which provides horizontal axis (X) data and a galvanometer which scans the vertical (Y) axis. It is also possible to image processes which takes place more quickly with the help of an electronic circuit tuner that enables us to image with 60 and 120 frames per second. The field of view is decreased in the vertical direction by one half of its full frame measurement for 60 frames and by one fourth for 120 frames per second. The frame rate capability of the two-photon microscope depends on the scanning rates of the galvanometer mirror.

The polygonal mirror composed of a disc with 36 facets equally distributed along the edge and rotating at a constant rate of 480 cycles each second. Each line in the image parallel to the horizontal axis is related with each facets and the scanning rate for the polygonal mirror is 17280 Hz. Lines per image corresponding to different frame rate can be calculated while keeping the polygonal mirror fixed and varying the galvanometer frequency f_g

$$N = \frac{17280\ Hz}{f_g}, \tag{1.35}$$

Table 1.1 - Lines per image corresponding to different frame rates.

Frame Rate $\boldsymbol{f_g}$ (Hz)	Lines per image N
30	576
60	288
120	144

The galvanometer and polygonal mirror is synchronized by using a bi-cell photodiode which counts the number of lines formed by the polygonal mirror and produce an electronic sign that drives the galvanometer at a particular frequency. The synchronization signal is formed by

utilizing a 650 nm laser diode that reflects off the rotating polygonal mirror and the reflection is scanned over the bi-cell photodiode.

1.4.4 DICHROIC MIRRORS

Laser lights of different wavelength can be separated by using a dichroic mirror. Dichroic mirrors has the property to transmitting a specific range of wavelengths and reflecting the rest. In our framework we utilized three dichroic mirrors and the first one reflects all wavelengths except for lights with wavelengths above 660 nm enabling the excitation light to pass through. The excitation light excites the sample and the fluorescent radiated by the sample is reflected in a perpendicular direction with the initial light to the detectors. The dichroic mirror b transmits beam of wavelengths above 520 nm and reflecting any light with wavelengths bellow that value toward the blue channel. The next dichroic reflects any light of wavelengths bellow 580 nm to the green channel and transmits anything above that towards the red channel detector.

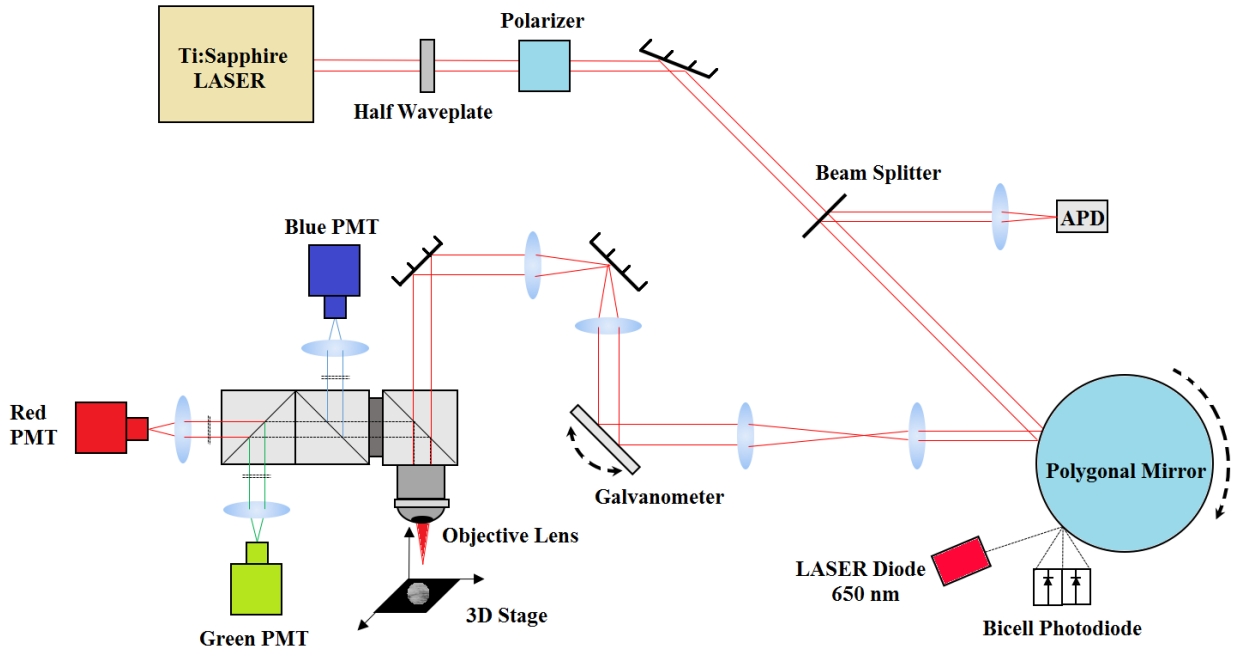

Figure 1.5 - Schematic of Two-Photon Fluorescence Microscope developed at UTEP

1.4.5 BANDPASS FILTERS

The bandpass filters filter beam of light with frequency outside the passband while transmitting light within the passband resulting a narrow frequency spectrum. In our two-photon microscope there are three pairs of bandpass filters. We used pairs of bandpass filter to strongly filter the light before reaching the detection channel. We used filters of 483 nm for blue detection channel, 542 nm for green and 624 nm for red detection channel. These filters narrow the frequency spectrum collected by the three detection channel by transmitting specific range of frequencies.

1.4.6 OBJECTIVE LENS

In our two-photon microscope framework there are objective lenses which have different numerical aperture (NA) and working distances. Objective lens is mainly responsible for exciting the sample through focusing the incoming light and collecting the radiated light from the sample.

Numerical aperture (NA) is an embedded property of the objective lens that characterize the dimensionless measurement of a range of angles for which the objective lens can transmit and acknowledge light. It is defined as

$$NA = n \sin \beta, \tag{1.36}$$

Here n is the index of refraction of the objective immersion liquid and β is the half angle of the maximum cone of light that the objective lens can acknowledge and transmit and these parameters can determine the working distance of the microscope and lateral resolution. When the sample is in sharp focus the working distance is defined as the separation between the objective lens and the nearest surface of the glass coverslip. Objective lens with a higher numerical aperture and magnification have a shorter working distance.

The property of the objective lens plays a vital role in deciding the resolution of a microscopic system. The optical sectioning is an inherent capability of our framework and that enables to do three dimensional imaging. Abbe's equation can be used to approximate the lateral resolution of the two-photon microscope

$$R = 0.6 \frac{\lambda}{NA} \approx \frac{\lambda}{2NA}, \tag{1.37}$$

Here R is defined as the minimum distance between the distinguishable objects and λ is the illuminating light wavelength. According to the equation the lateral resolution increases with higher numerical aperture (NA) since NA is inversely proportional to the minimum distance. Therefore to improve the resolution a higher NA objective lens should be used. On the other hand

a lower NA is required to achieve deeper penetration. In our lab we used mainly two objective lenses both are liquid (water) immersive with a magnification factor of 60X and numerical aperture of 1.0 and 1.2. For live fly brain imaging we used a wavelength of 850 nm and for such wavelength we got a lateral resolution of 0.51 μm and 0.425 μm for NA 1.0 and 1.2 respectively. It is clear that for a higher numerical aperture we got a better lateral resolution.

1.4.7 PHOTOMULTIPLIER TUBE (PMT)

In our two-photon fluorescence framework one of the most important part is the photomultiplier tubes. In our system the fluorescent light which is filtered using bandpass filters and dichroic mirrors is collected using photomultipliers tubes. Unique PMTs are used to collect separately the red, green and blue lights. The PMT is composed of photosensitive surface which can efficiently detect the incident of photons and can convert those detection into electronic signal by generating electronic charges that are amplified and sensed. The quantity of the photon captured by the photosensitive surface is the yield of the PMT. Photomultiplier tubes can detect the change of photon flux within a few nanoseconds and therefore are suitable for detection and recording of events which occurs really quickly. The quantum efficiency (QE) of these types of devices ranges between 20% and 40% which is the percentage of detected photons. The QE is a function of the illumination wavelength and it depends on the chemical composition of the surface.

In our setup, each PMT is connected with a Hamamatsu C7950 socket which can convert small current with high impedance output of the PMT into a low-impedance voltage output. The socket has a transformation factor of 0.3 V/μA. A variable power supply is connected with each C7950 socket that can be tuned from 0 V to +3.6 V. The high voltage adjustments is used to tune the gain of the amplification circuit.

One of the most important measurement which defines the performance of an electronic sensor is the signal to noise ratio. One of the most important property of the PMT is the high signal to noise ratio which is due to considerably low dark current. Dark current arises in the absence of light and is common for this type of sensors.

1.4.8 THREE DIMENSIONAL STAGE

Three dimensional stage provide the comfort of imaging 3D images of the sample as it is capable of moving in all three axes. The combination of the mounted galvanometer and turning polygonal mirror provide us the facility to produce two dimensional images for a fixed Z-axis position. To construct the three dimensional reconstruction of the sample it is required to image in different Z-position. The 3D motorized stage (Shutter Instrument, MP-285) used with our microscope is capable of travelling one inch in all the three axes and delivers a minimum resolution of 0.2 μm/step and high resolution of 0.04 μm/step with a maximum speed 2.9 μm/step. To image the live fly brain we typically used 1 μm/step between the planes along Z-axis.

1.5 ADVANTAGES OF TWO-PHOTON MICROSCOPY

Fluorophores are fluorescent compounds and when they are illuminated by a series of laser pulses through a focusing lens, the probability per pulse that a fluorophore will be excited by the two-photon absorption is

$$n_a \propto \frac{\delta_2 {P^2}_{ave}}{\tau_p {f^2}_p} \left(\frac{NA^2}{2\tau\delta\hbar c\lambda} \right)^2 \tag{1.38}$$

Here δ_2 is the two-photon cross section of the fluorophore with wavelength λ, NA is the numerical aperture of the focusing lens, $\hbar$ is the planks constant, c is the speed of light and P_{ave} is the average power of the laser beam [8].

In an experiment, the image start losing optical resolution if the saturation ($n_a \approx 1$) is not avoided and the resolution is defined by the excitation wavelength and the numerical aperture of the lens. To maximize the signal generation the pulse power and pulse width are also set accordingly.

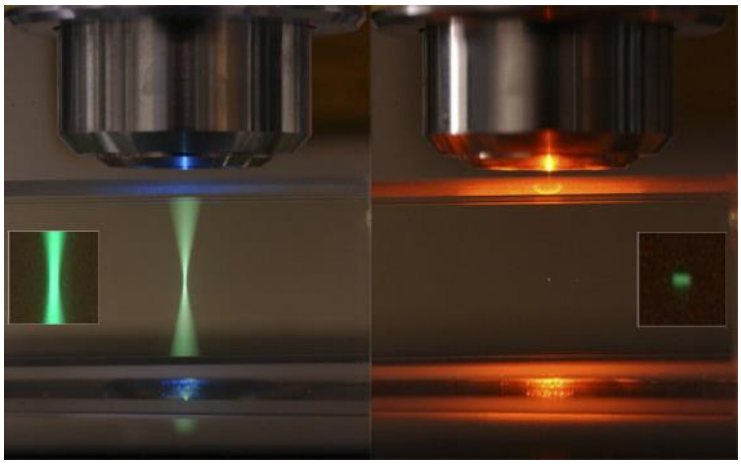

Figure 1.6 – Focal plane of single photon (left) Vs two-photon (right) fluorescence imaging microscopy [9].

In the two-photon microscope the fluorescence signal can be spatially confined by confining the excitation light due to the fact that the signal produced by two-photon microscope is proportional to the probability of the two-photon absorption and the procedure scales with the squared intensity of the laser. One of the key advantages of TPM is the signal acquisition from a small section of the sample. The light cone in TPM is largest at the focal plane and rapidly dies off in the regions around. It is demonstrated in Figure 1.7 by comparing the effect of one- and two-photon absorption on signal generation.

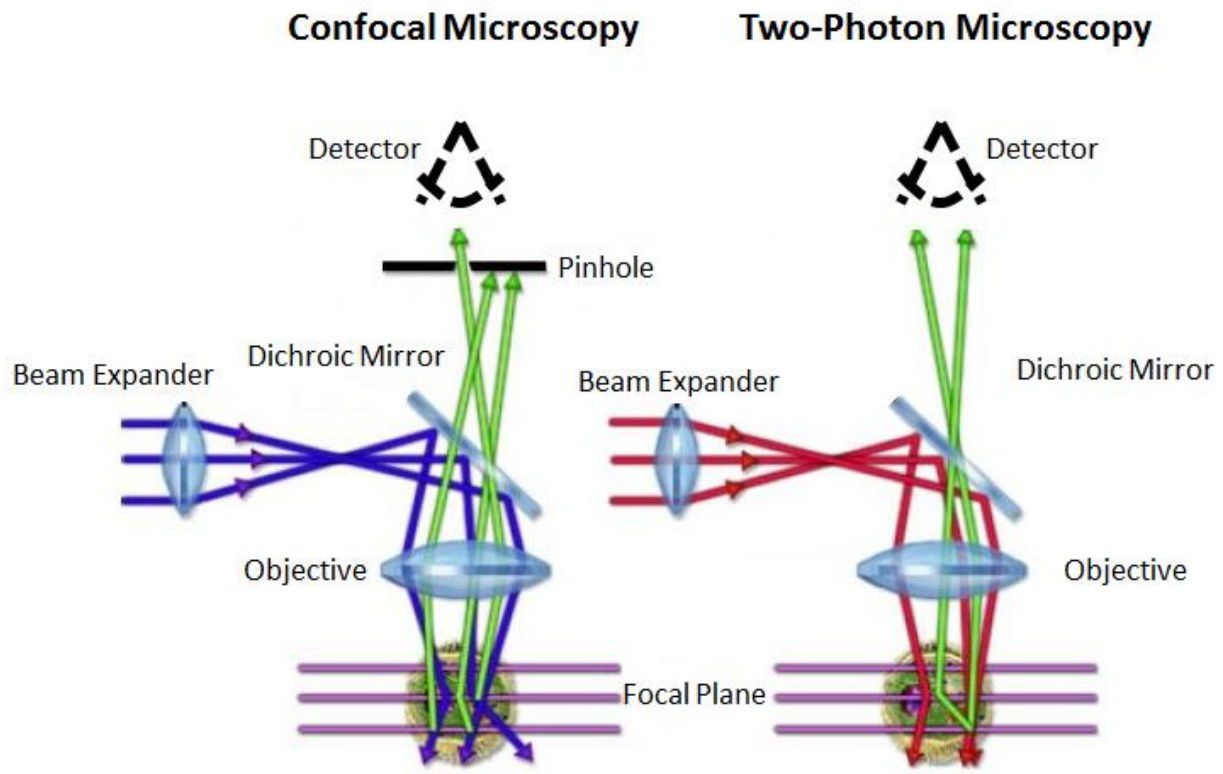

Figure 1.7 – Comparison between confocal microscopy and two-photon microscopy.

Optically thick specimen are very important samples that needs to be analyzed to find out important information about protein interactions. Resolving microscopic structure in optically thick specimens is limited in conventional light microscopy because the image gets blurred at the focal plane by the out of focus noise.

Three dimensional imaging is an important imaging tool and it has been realized after the invention of confocal microscopy and two-photon microscopy. Both confocal and two-photon microscopy are really similar in imaging technique. In confocal microscope there are a set of conjugate apertures to achieve 3D resolution. Among those apertures, one of them is to illuminate the sample and the other for detecting the fluorescent light and scatterings [10] These apertures

ensure that the microscope illuminate and detect from the same volume within the sample by functioning as spatial filters.

An additional benefit of TPM is the ability to image exceedingly heterogeneous thick samples which is due to the use of wavelengths near IR region relative to wavelengths in visible and UV spectrum used in conventional fluorescence microscopy. With proper objectives and since light scattering is proportional to λ^{-4}, TPM has been used to image biological events up to several hundred microns within condensed tissues [11]. The high penetration depth of TPM is further improved because most biological samples present minute linear absorption between 700 and 1000 nm.

CHAPTER 2: LIVE IMAGING OF DROSOPHILA MELANOGASTER BRAIN USING TWO-PHOTON MICROSCOPY

2.1 INTRODUCTION

Cyclic adenosine monophosphate (cAMP) is responsible for intra-neural signal transduction [12]. Cyclic AMP is produced when the level of dopamine is altered and it is responsible for the cognition processes. Dopamine is an important neurotransmitter in the nervous system and is released to communicate signals between neuron cells. In humans, abnormality in dopamine level is associated with different diseases. To shed light on the cAMP functioning mechanism, we investigate the Drosophila melanogaster brains *in vivo*. The neural assembly of interest is the mushroom body which is accountable for the basic operations of olfactory learning and memory and contains dopamine receptors. We used Drosophila melanogaster due to its short life span and fast biological processes. Additionally, it is considered as a typical organism for biological queries. To measure the effect of varying dopamine levels on cAMP production, fluorescence resonance energy transfer (FRET) technique is used along with exchange proteins which are activated by cAMP (EPAC). FRET is a distance reliant non-radiative transfer of energy between an excited and suitable D-A pair of fluorophores. The mechanism of FRET when applied to optical microscopy, permits to define the distance between two fluorophore molecules within several nanometers and is considered as one of the few tools accessible for assessing the changes in nanometer scale. The Fluorescence Resonance Energy Transfer (FRET) between two molecules is a significant physical phenomenon with substantial interest for understanding biological systems [13].

2.2 FÖRSTER RESONANCE ENERGY TRANSFER (FRET)

Förster Resonance Energy Transfer (FRET) is named after the physicist and it has become an important tool for investigating molecular structure and dynamics. FRET is particularly used in probing protein interactions and cell signaling pathways [14]. According to the theory of FRET it represents the non-radiative energy transfer from an excited fluorescent protein called the donor to an acceptor which is another fluorophore. This interaction take place in a close proximity typically within 10 nm. Therefore using the principle of FRET it is possible to excite the acceptor fluorophores just by exciting the donor fluorophores which will in turn excite the acceptors with a non-radiative transfer of energy. Although there are few conditions which must has to meet for FRET to take place and these conditions can briefly describes as:

1. Close proximity of the fluorophores typically <10 nm

2. Overlapped spectra of the donor emission and acceptor excitation

3. The fluorophores should be oriented in a non-orthogonal orientation.

2.3 PRINCIPLE OF FRET

The mechanism of FRET comprises a fluorophore in excited electronic state, the donor which transfer energy in a non-radiative process to another fluorophore, the acceptor in close proximity. One of the key advantages of non-radiative process is that it can achieve significant information about the donor-acceptor par structure. Unlike radiative mechanism, FRET does not depends on optical properties and dimension of the specimen. FRET is independent of the wave-front pathways and does not requires emission as well as reabsorption of a photon.

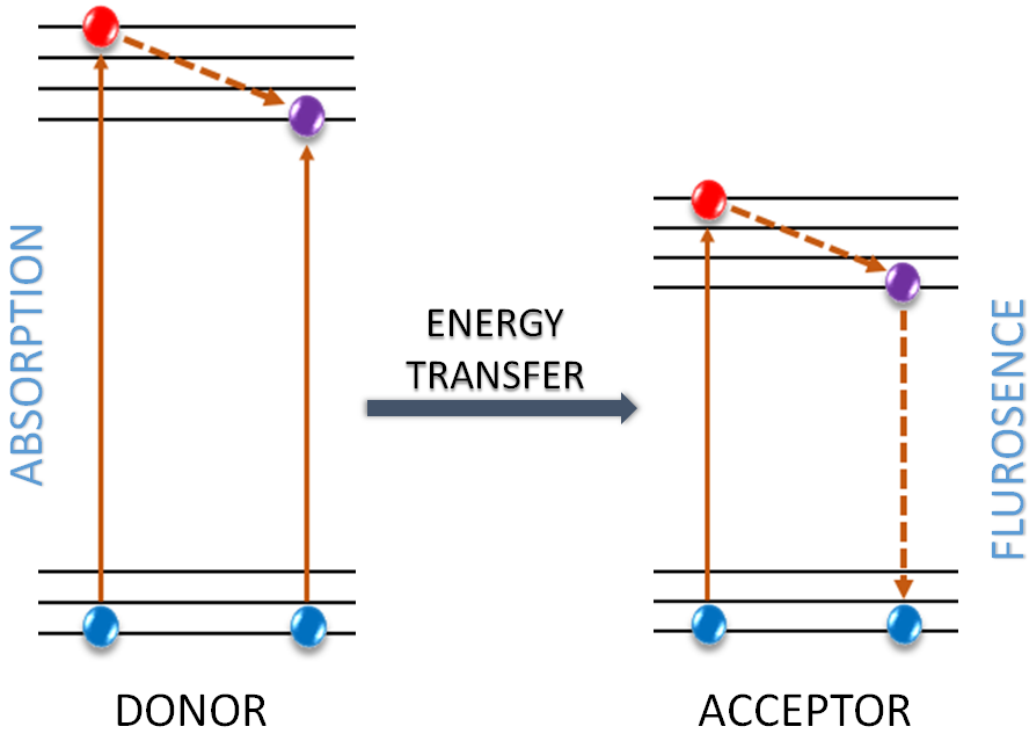

Figure 2.1: Jablonski diagram illustrating FRET for TPE

Resonance energy transfer yields unique molecular data to that discovered by events which are solvent dependent like the fluorescence quenching, anisotropic measurements and excited state reactions since it is not sensitive to the solvent shell surrounding a fluorophore. The effect on the spectral properties of the donor and acceptor is the major solvent impact on fluorophores undergoing resonance energy transfer. Resonance energy transfer depends on the distance between the donor and the acceptor and the non-radiative energy transfer occurs over longer distances unlike the short range solvent effects therefore the dielectric nature of the solvent as well as other elements residing between the involved fluorophores has very little influence on the efficiency of resonance energy transfer.

Treating the donor as a dipole $\overrightarrow{\mu_D}$ radiating at frequency ω_0 and the acceptor as a dipole $\overrightarrow{\mu_A}$, the energy transfer rate may be given by

$$\gamma_{D\to A} = \frac{1}{\tau_D}\frac{P_{D\to A}}{P_o}, \tag{2.1}$$

where τ_D is the fluorescence lifetime of the isolated donor, $P_{D\to A}$ is the donor's energy per unit time which is absorbed by the acceptor, and P_0 is the energy per unit time released from the donor in absence of the acceptor, P_0 can be written as

$$P_0 = \frac{|\overrightarrow{\mu_D}|^2 n(\omega_0)}{12\pi\epsilon_0 c^3}{\omega_0}^4. \tag{2.2}$$

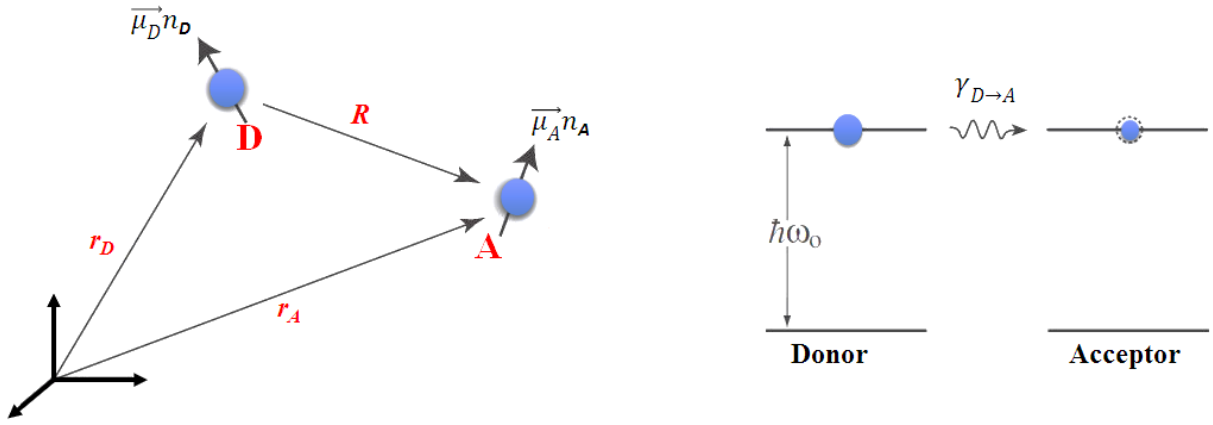

Figure 2.2: Energy transfer between a D-A pair where at the beginning the donor (D) is an excited state and the acceptor (A) is in ground state.

According to the Poynting's theorem the power transferred from donor to acceptor is

$$P_{D\to A} = -\frac{1}{2}\int_{VA} Re\left\{\overrightarrow{J_A^*}\cdot\overrightarrow{E_D}\right\}dV, \tag{2.3}$$

Here $\overrightarrow{J_A}$ is the current density associated with the acceptor charges and $\overrightarrow{E_D}$ is the electric field generated by the donor. In the dipole approximation, the current density can be given by

$$\overrightarrow{J_A} = -i\omega_0\overrightarrow{\mu_A}\delta(\vec{r} - \overrightarrow{r_A}), \tag{2.4}$$

thus Eq. (2.3) may be reduced to

$$P_{D\to A} = \frac{\omega_0}{2} Im\left\{\overrightarrow{\mu_A^*}\cdot\overrightarrow{E_D}(\overrightarrow{r_A})\right\}. \tag{2.5}$$

The dipole moment $\overrightarrow{\mu_A}$ is not a permanent dipole moment because it is the dipole induced by the field generated by the donor, therefore dipole moment of the acceptor can be written as

$$\overrightarrow{\mu_A} = \alpha_A\overrightarrow{E_D}(\overrightarrow{r_A}), \tag{2.6}$$

where α_A is the polarizability tensor of the acceptor. Assuming the polarization of the acceptor is fixed and given by the unit vector $\widehat{n_A}$,

$$P_{D\to A} = \frac{\omega_0}{2} Im\{\alpha_A\}\left|\widehat{n_A}\cdot\overrightarrow{E_D}(\overrightarrow{r_A})\right|^2. \tag{2.7}$$

Since $\overrightarrow{\mu_A}$ is a induced dipole it is convenient to write the polarizability in term of the absorption cross-section σ_A,

$$\sigma_A(\omega_0) = \frac{\langle P(\omega_0)\rangle}{I(\omega_0)}, \tag{2.8}$$

where $\langle P(\omega_0)\rangle$ is the acceptor absorbed power averaged over all dipole orientations and $I(\omega_0)$ is the incident intensity. In terms of electric field it can be written as,

$$\sigma_A(\omega_0) = \frac{(\omega_0/2) Im\{\alpha_A(\omega_0)\}\,\langle\left|\hat{n}\cdot\overrightarrow{E_D}\right|^2\rangle}{(1/2)\sqrt{\epsilon_0/\mu_0}\, n(\omega_0)\left|\overrightarrow{E_D}\right|^2}. \tag{2.9}$$

Taking the orientational average of $\langle\left|\hat{n}\cdot\overrightarrow{E_D}\right|^2\rangle$,

$$\langle\left|\hat{n}\cdot\overrightarrow{E_D}\right|^2\rangle = \frac{\left|\overrightarrow{E_D}\right|^2}{4\pi}\int_0^{2\pi}\int_0^{\pi}[\cos^2\theta]\sin\theta\, d\theta\, d\phi = \frac{1}{3}\left|\overrightarrow{E_D}\right|^2, \tag{2.10}$$

where θ is the angle between the dipole axis and the electric field vector. Therefore the power transferred between the donor and acceptor can be given by

$$P_{D\to A} = \frac{3}{2}\sqrt{\frac{\epsilon_0}{\mu_0}}\, n(\omega_0)\sigma_A(\omega_0)\left|\widehat{n_A}\cdot\overrightarrow{E_D}(\overrightarrow{r_A})\right|^2. \tag{2.11}$$

The donor's field $\overrightarrow{E_D}$ evaluated at the origin of the acceptor r_A and may be modeled by the electric field of a dipole,

$$\overrightarrow{E_D}(r_A) = \frac{1}{4\pi\epsilon_0}\frac{1}{r^3}[3(\overrightarrow{\mu_D}\cdot\widehat{n_r})\widehat{n_r} - \overrightarrow{\mu_D}], \tag{2.12}$$

where $\vec{r} = r\widehat{n_r}$ is the vector from the acceptor to the donor. The donor's dipole moment can be represented as

$$\overrightarrow{\mu_D} = |\overrightarrow{\mu_D}|\widehat{n_D}, \tag{2.13}$$

therefore using this equation in Eq. (2.12) yields,

$$\overrightarrow{E_D}(r_A) = \frac{1}{4\pi\epsilon_0}\frac{\mu_D}{r^3}[3(\widehat{n_D}\cdot\widehat{n_r})\widehat{n_r} - \widehat{n_D}], \tag{2.14}$$

substituting Eq. (2.14) in Eq. (2.11),

$$P_{D\to A} = \frac{3{\mu_D}^2}{32\pi^2}\frac{\sigma_A(\omega_0)}{n(\omega_0)}\frac{c}{\epsilon_0 r^6}[3(n_D\cdot n_r)(n_A\cdot n_r) - n_A\cdot n_D]^2. \tag{2.15}$$

The energy transfer dependence on the dipole orientation is generally written as

$$\kappa^2 = [3(n_D\cdot n_r)(n_A\cdot n_r) - n_A\cdot n_D]^2$$

Substituting it in Eq. (2.15) gives,

$$P_{D\to A} = \frac{3{\mu_D}^2}{32\pi^2}\frac{\sigma_A(\omega_0)}{n(\omega_0)}\frac{c\kappa^2}{\epsilon_0 r^6}. \tag{2.16}$$

The energy transfer rate is given by the ratio of $P_{D\to A}$ and P_0. We must consider using a normalized frequency distribution f_D if we take in account that the donor may radiate energy over a range of frequencies,

$$\frac{P_{D\to A}}{P_o} = \frac{9c^4\kappa^2}{8\pi r^6}\int_0^\infty \frac{\sigma_A(\omega)f_D(\omega)}{\omega^4 n^4(\omega)}d\omega \tag{2.17}$$

By substituting Eq. (2.17) into Eq. (2.1), the energy transfer rate is given as

$$\gamma_{D\to A} = \frac{1}{\tau_D}\frac{9c^4\kappa^2}{8\pi r^6}\int_0^\infty \frac{\sigma_A(\omega)f_D(\omega)}{\omega^4 n^4(\omega)}d\omega, \tag{2.18}$$

2.3.1 THE RATE OF ENERGY TRANSFER k_T

The rate of energy transfer between a donor and an acceptor was given by Förster in the form

$$k_T = \frac{1}{\tau_D}\left(\frac{R_0}{r}\right)^6, \tag{2.19}$$

Where τ_D is the fluorescence lifetime of the donor in absence of the acceptor and r is the distance btween the particular D-A pair. The Förster constant R_0 is a distance parameter and measured from the spectroscopic and shared dipole orientation parameters of the D-A pair κ^2 and given by

$$R_0{}^6 = \frac{9c^4\kappa^2}{8\pi}\int_0^\infty \frac{\sigma_A(\omega)f_D(\omega)}{\omega^4 n^4(\omega)}\,d\omega \tag{2.20}$$

The Förster constant R_0 is also associated with the spectral overlap integral of the D-A pair which is given by,

$$J = \int_0^\infty \frac{\sigma_A(\omega)f_D(\omega)}{\omega^4 n^4(\omega)}\,d\omega. \tag{2.21}$$

2.3.2 ENERGY TRANSFER EFFICIENCY *E*

The efficiency of the energy transfer is described by Förster as the number of photons absorbed by the donor that are transferred to the acceptor. It can be expressed as the ratio of rate of energy transfer k_t to the total decay rate of the donor

$$E = \frac{k_t}{k_t + \frac{1}{\tau_D}}. \tag{2.22}$$

Substituting Eq. (2.19) into Eq. (2.22) we obtain the relation between the efficiency of the energy transfer, Förster constant and the separation between the particular D-A pair

$$E_{FRET} = \frac{R_0{}^6}{R_0{}^6 + r^6}. \tag{2.23}$$

Bellow is a graph of Eq. (2.23). From the plot it is clear that the efficiency drastically drops as the distance between the D-A pair increases from the Förster constant. The efficiency has a major change from the point when it is equal to the Förster constant.

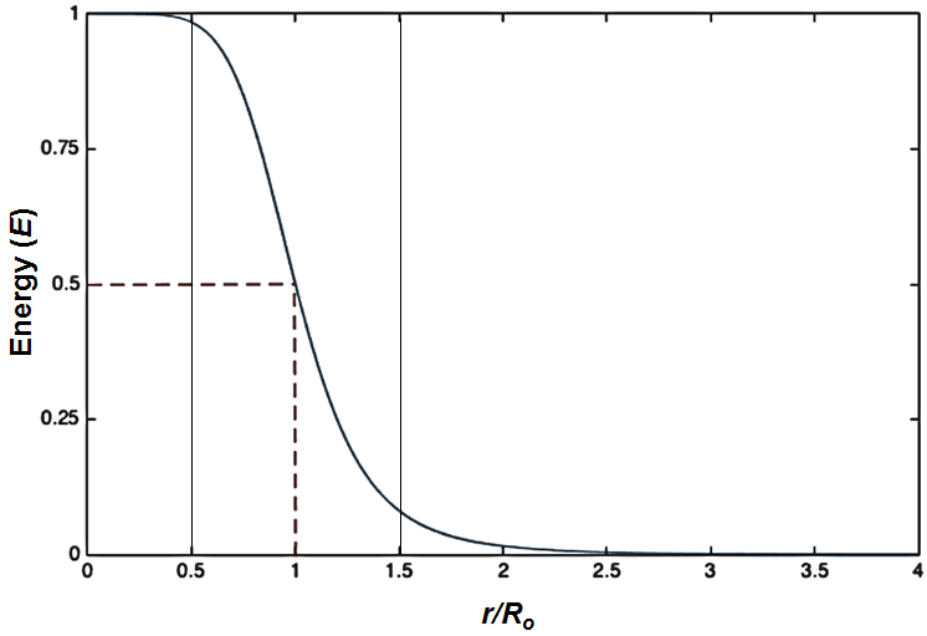

Figure 2.3: FRET efficiency plot.

2.3.4 ORIENTATION FACTOR κ^2

The orientation factor $\kappa^2 = [3(n_D \cdot n_r)(n_A \cdot n_r) - n_A \cdot n_D]^2$ defines the orientation of a D-A pair dipoles. The value of κ^2 can range from 0 to 4 which depends on the relative orientation of the dipole pairs. In case of both the dipoles oriented along the axis which separate them, the value of $\kappa^2 = 4$ and is known as the optimal configuration. In case of the optimal configuration all the vectors are parallel to each other. In most of the cases the orientation of the dipoles are unknown and to simplify the calculations κ^2 is assumed constant for all dipole configurations and the expectation value is $\langle \kappa^2 \rangle = \frac{2}{3}$. Systems with constant value of x are those considers fast

rotational dynamics of the dipoles associated and does not apply to the systems where the movement of the involved dipoles are restricted.

2.3.4 SPECTRAL OVERLAP INTEGRAL

The spectral integral $J(\lambda)$ can be expressed as a function of wavelength which gives the amount of spectral overlap between the acceptor and the donor. It can be expressed in the form

$$J(\lambda) = \int_0^\infty f_D(\lambda)\varepsilon_A(\lambda)\lambda^4 d\lambda \tag{2.24}$$

where $f_D(\lambda)$ is the normalized form of the donor fluorescence spectra and $\varepsilon_A(\lambda)$ is called the extinction coefficient of the acceptor at λ. The extinction coefficient is an intrinsic property of the fluorophore which measures the strength of acceptor of absorbing photon unlike $f_D(\lambda)$ which depends on the fluorophore surroundings and therefore the spectral overlap integral depends on the medium. The spectral overlap integral can be expressed as the overlap of the donor emission spectra and the acceptor absorption spectrum shown in Figure (2.4).

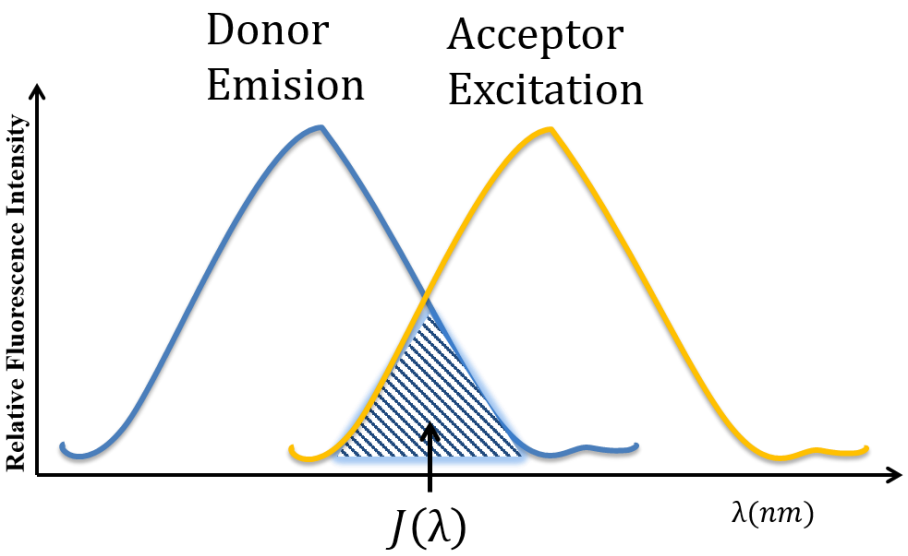

Figure 2.4: Emission and absorption spectra of D-A pair

2.4 CYCLIC ADENOSINE MONOPHOSPHATE (cAMP)

Cyclic adenosine monophosphate (cAMP) is a second messenger molecule and it is a derivative of adenosine triphosphate (ATP) as shown in Figure (2.1). Cyclic AMP is produced from ATP by adenylate cyclase located on the internal portion of the plasma membrane and attached at various locations in the interior of the cell [15]. The adenylyl cyclase is a first messenger and is triggered after the ligation of G protein coupled receptors by ligands including prostaglandis, autocoids, hormones and pharmacologic agents. The signals produced by the adenylyl cyclase is responded by cells by releasing cAMP. Cyclic AMP is associated with almost all the cellular process which includes cell division and growth, gene expression, neurotransmission and metabolism. cAMP is also responsible for triggering physiological processes such as memory and learning, relaxation and kidney water uptake [16]. Cyclic AMP is also involved in activating protein kinases, regulating function of ion channels and other cyclic-nucleotide proteins.

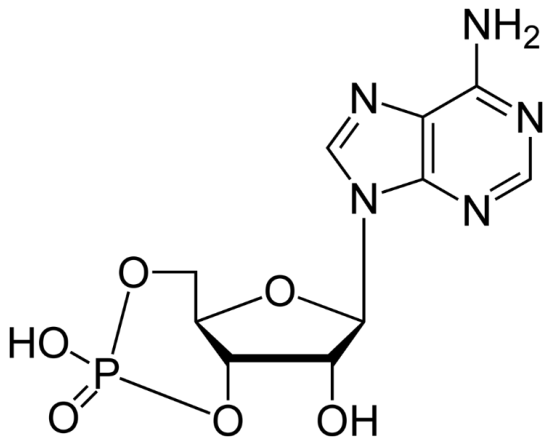

Figure 2.5: 2D skeletal formula of cAMP [17]

2.5 DOPAMINE (DA)

Dopamine (DA) is an organic chemical compound contacted from 3,4 dihydroxyphenethylamine). Dopamine is synthesized from amine through removing carboxyl group from L-DOPA molecule. Synthetization of dopamine is common in brain, kidney as well as plants and animals.

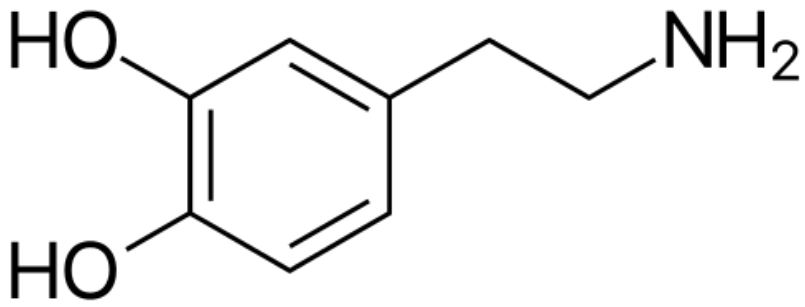

Figure 2.6: 2D skeletal formula of dopamine [18]

Dopamine is one of the major neurotransmitters of central and peripheral nervous system which is released by nerve cells to communicate with each other. Neurotransmission due to

dopamine is very important due to its connection with cognitive degeneration [19]. Dopamine has been connected to cognitive aging as well as reduced cognitive function irrespective of age [20]. Reward motivated behavior plays a major role among the distinct dopamine pathways and cause an increase in dopamine neural activity. Besides, other dopamine pathways are involved in motor control and regulating hormones. Additionally, patients diagnosed with Huntington's disease, schizophrenia and Parkinson's disease show irregular dopamine function.

2.6 FLUOROPHORES (CFP-YFP PAIRS)

Fluorophores are fluorescent chemical compound which comprises several collective aromatic clusters. Additionally, they can also composed of planar or cyclic molecules with several π bonds. Fluorophores absorbs light energy of a specific wavelength and are capable of re-emitting light after they are excited. In our experiment the targeted fluorophores are a pair of fluorophores which is most commonly used for biological queries [21], cyan fluorescent protein (CFP) and yellow fluorescent protein (YFP). CFP acts as a donor and YFP behaves as an acceptor. CFP and YFP are color variants of green fluorescence protein (GFP). The absorption and emission spectra of these fluorophores is well recognized [22]. In case of CFP-YFP pair, it is possible to excite both fluorophores by only exciting the CFP fluorophore due to their overlapping spectra under two-photon absorption. Since CFP emission spectra overlaps with the YFP absorption spectra therefore just by exciting CFP will in turn excite the YFP fluorophore through FRET.

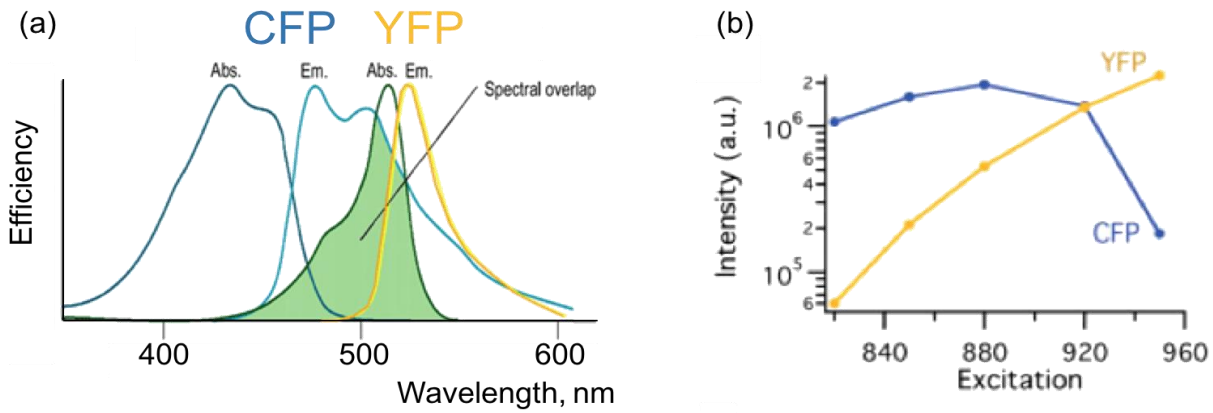

Figure 2.7 – (a) CFP and YFP spectral overlap with one-photon absorption,

(b) Intensity of CFP and YFP emission for different TPE excitation wavelengths [22]

In Figure (2.7a), the overlap between the CFP emission spectra and YFP absorption spectra is highlighted in green and it shows an insignificant overlap range. From Figure (2.7b) it is seen that the fluorescence intensity of CFP fluorophore is maximum for 880nm excitation wavelength with TPE. The intensity for YFP fluorophore at 880nm wavelength is not ideal for FRET since it can increase the probability of direct excitation and may decrease the success rate of FRET. The ideal wavelength for FRET to occur successfully has been found to be 850nm because at this wavelength the intensity of YFP fluorophore is one-fifth of CFP fluorophore which significantly reduce the probability of direct excitation and can produce YFP fluorescence due to indirect excitation through CFP excitation.

2.7 EXCHANGE PROTEIN DIRECTLY ACTIVATED BY CYCLIC AMP (Epac1)

Epac is a novel cAMP sensor [23, 24]. These type of proteins contain cAMP binding domain (CBD) [25] and can bind with cAMP with high affinity. There are Epac1 and Epac2 which are two isoforms of Epac where Epac1 is universally distributed in all tissues [23, 24]. In our study

we used Epac1 and as shown in Figure (2.8), in absence of cAMP, Epac is folded in such a way that the CFP-YFP fluorophore are close to each other so that FRET can occur. When cAMP is released due to the stimulant, Epac gets activated by cAMP and the protein unfolds causing the fluorophore pairs to move away from each other resulting low FRET [26].

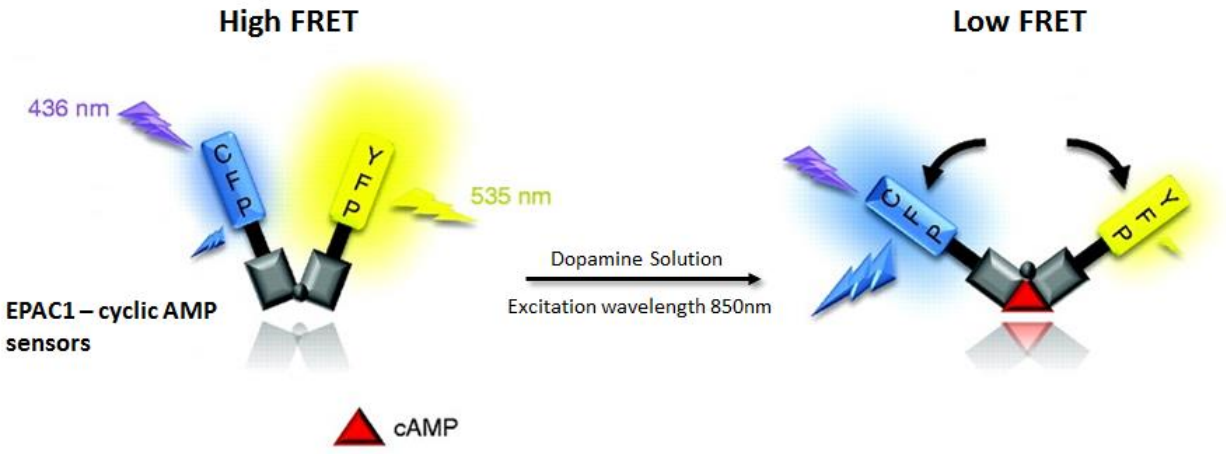

Figure 2.8 – cyclic AMP dependent Epac1 configuration.

2.8 TWO-PHOTON IMAGING OF LIVE DROSOPHILA BRAIN USING FRET FOR cAMP DYNAMICS

2.8.1 SAMPLE PREPARATION

Drosophila melanogaster is a species of fly commonly known as the fruit fly. D. melanogaster is widely used in biological research such as genetics, microbial pathogenesis, life history evolution and physiology due to that fact that it can quickly breed, has a short life span and they are readily raised in the laboratory [27]. In our experiment we used GAL4 MB247 fly batch which are 4-7 days old adults. The sample preparation can listed as follows:

- Immobilizing flies on ice and gluing them inside a cylindrical hole situated at the center of a round slide using two percent agarose solution.
- A small window was cut open into the live drosophila head under an optical microscope and trachea was removed from that region.
- The sample was bathed with hemolymph like saline solution which protects the brain and ensure essential nutrients for the fly.

Agarose is a polymer material which is extracted from seaweed and is frequently used in molecular biology. Agarose is made up from repeating units of agarobiose and is a linear polymer [28]. Below Table (2.1) and (2.2) shows the composition of hemolymph and dopamine solution.

Table 2.1 – Composition of hemolymph like saline

Hemolymph-like saline (HL3)	
NaCl	70 mM
KCl	5 mM
$CaCl_2$	1.5 mM
$MgCl_2$	20 mM
$NaHCO_3$	10 mM
Trehalose	5 mM
Sucrose	115 mM
Hepes, pH 7.1	5 mM

Table 2.2 – Composition of dopamine solution, molecular weight and preparation of 1mM concentration

	F.W.	Molar Concentration	Amount
Dopamine	189.64 g/mol	1 mM	1 ml
	Aliquots of 500 mM concentration into 10µl Then 1µl in 499 µl of HL3= 1mM concentration 2µl in 998 µl HL3 =1mM concentration; 1 ml amount		

2.8.2 EXPERIMENTAL METHOD

Live Drosophila melanogaster fly is immobilized on ice and glued onto a slide using agarose solution. A small window was cut into the head capsule and the brain was bathed with hemolymph solution. Hemolymph is a saline like solution which protect the brain and preserve brain functions. The preparation was placed under a two-photon fluorescence microscope with 720nm excitation wavelength equipped with a 70X water immersion objective lens. At 720nm it is efficient to locate the sample and after locating the fly under the microscope, the wavelength is changed to 850nm. Image acquisition was done at different z-positions each 1 µm apart within the sample's mushroom body. The experiment was divided into two phases where Phase I corresponds to the baseline and Phase II corresponding the effect of dopamine in cAMP dynamics. To determine the baseline the experiment was carried out with saline solution only. The brain is scanned while bathed in saline solution with the two-photon microscope. In the next phase of the experiment the laser was blocked to reduce photo bleaching and the saline solution is washed out. After washing the saline solution the brain is stimulated by bathing with 1mM dopamine solution applied using a micropipette and then scanned again. The injection of the dopamine solution

caused a drop in fluorescence intensity which may perhaps due to the change in refractive index of the solvent .The process is depicted in Figure (2.9)

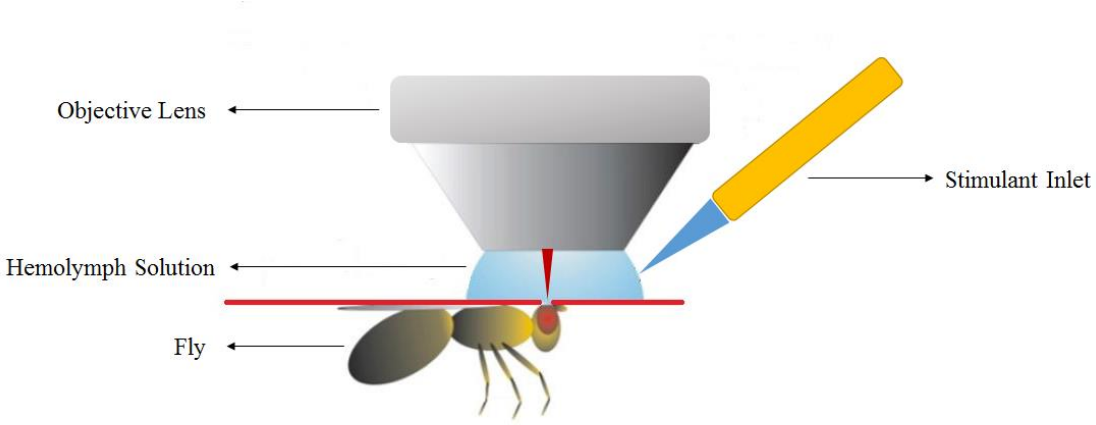

Figure 2.9 – Schematic illustration of *in vivo* preparation

The images were taken using the green PMT to collect the fluorescent signal of the YFP and blue PMT for CFP signal. The laser power was 200 mW and the PMT voltages were set to 2.15 V. For our experiment we used 542 nm dichroic and 580 nm filter for green channel and 483 nm dichroic and 520 nm for blue channel. Image processing was carried out using the software ImageJ.

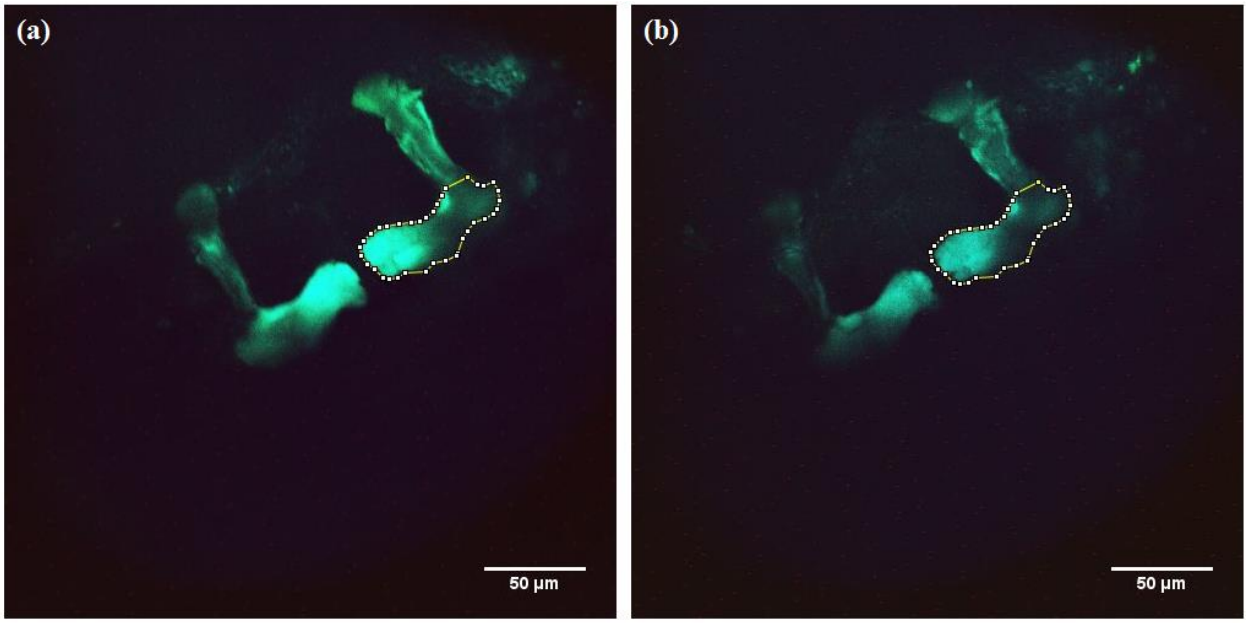

Figure 2.10 – Mushroom bodies with targeted region (γ-lobe) a) bathed in hemolymph like solution

b) Washed and again bathed with dopamine solution

2.8.3 IMAGE PROCESSING USING IMAGEJ

Image acquired using the two-photon microscope were processed, measured and the data was stored using ImageJ software where each of the RGB TIF files contain values in green and blue channel. The step by step process can be listed as:

- The RGB image was split into grayscale green and blue channel.
- For rendering purposes the green channel signal was given yellow color and blue channel signal was set to cyan color which corresponds YFP and CFP signals respectively.
- Selection tool was used to measure the highlighted region.
- Measurement was carried-out using the ImageJ inbuilt measurement tool and the data was saved as an excel file.

2.8.4 RESULTS

During the first part of our experiment, we have excited the sample with 850 nm excitation wavelength and scanned the mushroom bodies inside a Drosophila brain *in vivo*. At the beginning we used hemolymph like solution to bath the brain. During the phase II of our experiment we washed out the solution and again excited it with the same wavelength, bathed the sample with dopamine solution and rescanned. Below Figure (2.11) shows the CFP and YFP signal before and after administering dopamine solution. From the scanned images the fluorescence intensity of the γ-lobes were analyzed. Besides the background intensity of each different Z-position was also measured, analyzed and subtracted from the previous signals.

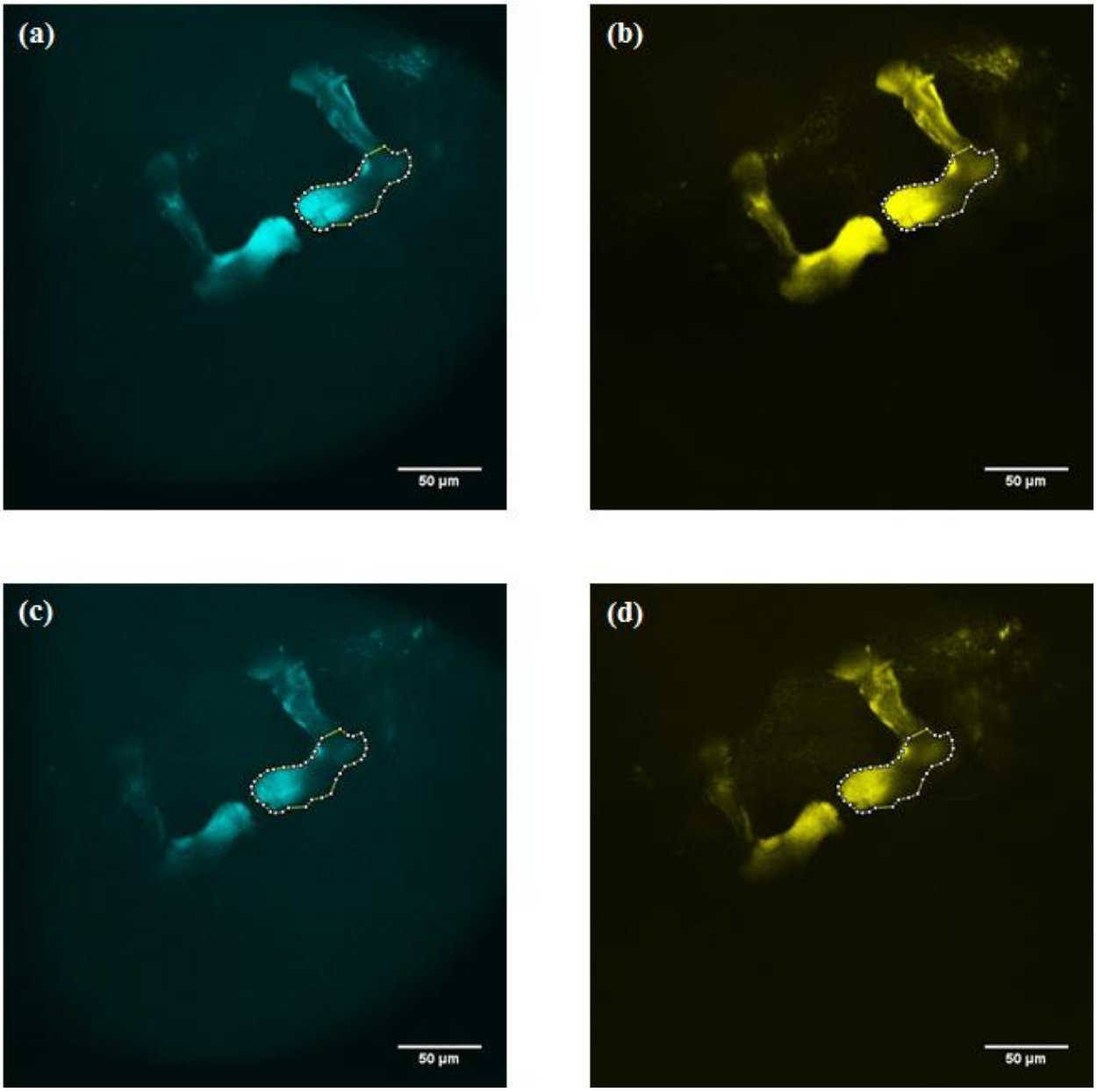

Figure 2.10 – a) CFP b) YFP signal from the mushroom bodies before administering dopamine and c) CFP d) YFP signal from the mushroom bodies after administering dopamine.

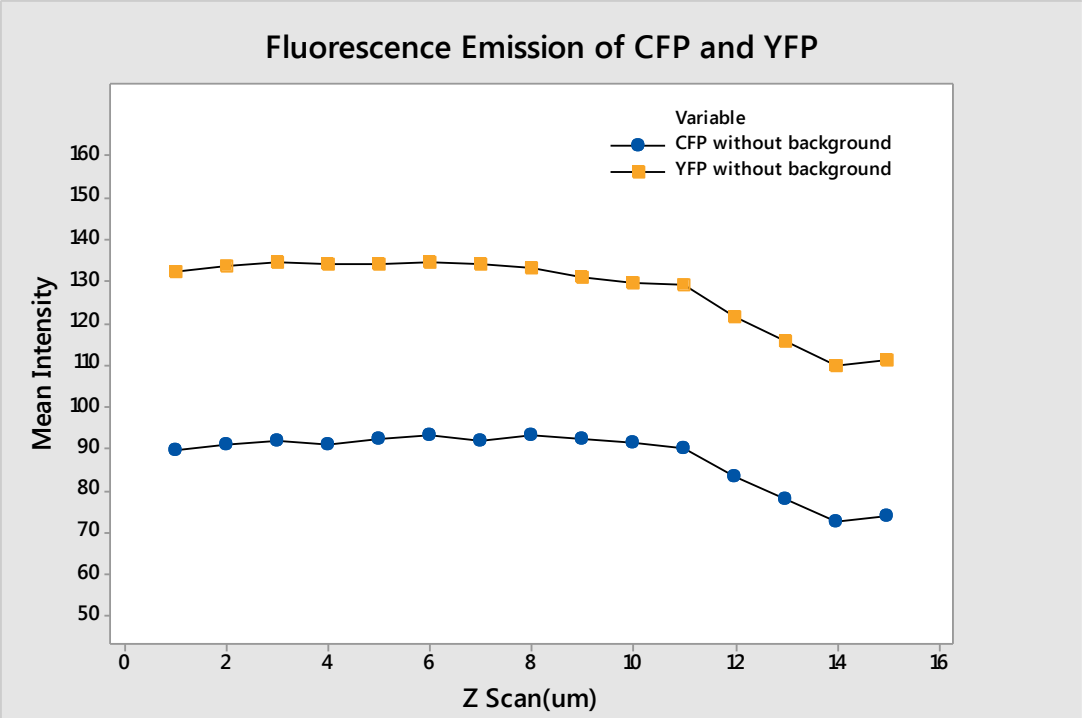
Fluorescence Emission of CFP and YFP
Variable
CFP without background
YFP without background
Mean Intensity
160
150
140
130
120
110
100
90
80
70
60
50
0
2
4
6
8
10
12
14
16
Z Scan(um)

(a)

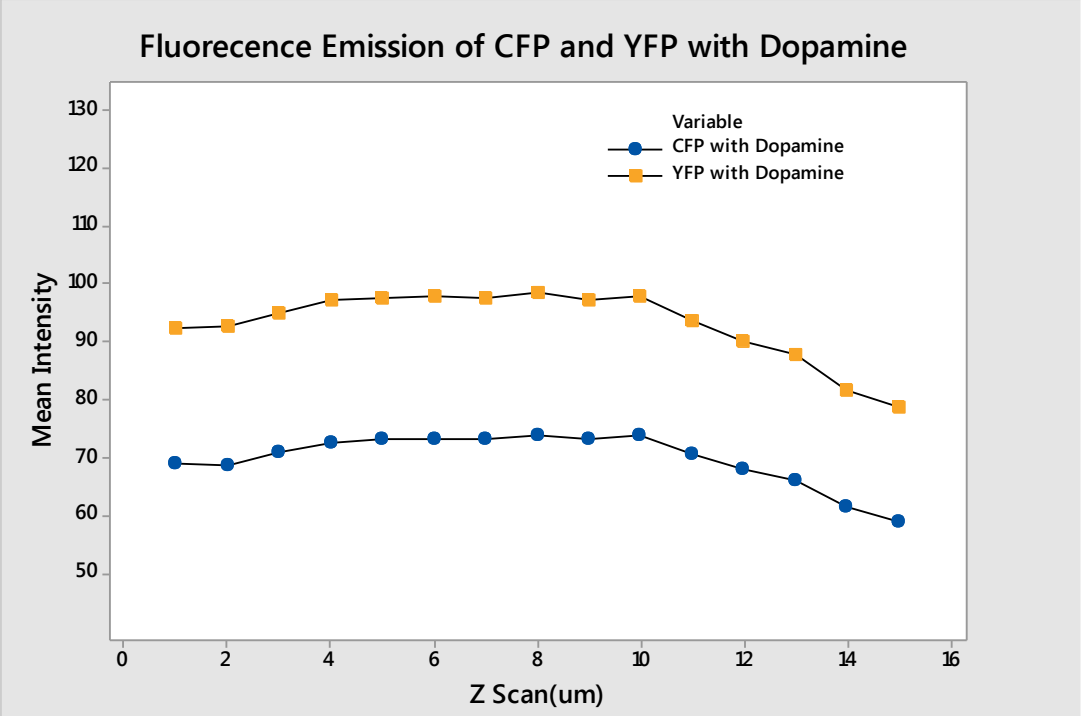
Fluorecence Emission of CFP and YFP with Dopamine
Variable
CFP with Dopamine
YFP with Dopamine
Mean Intensity
130
120
110
100
90
80
70
60
50
0
2
4
6
8
10
12
14
16
Z Scan(um)

(b)

Figure 2.12 (a) (b) – Fluorescence emission level of CFP and YFP before and after administering dopamine

Figure (2.12) shows a drop in intensity level for both CFP and YFP fluorescence intensity after adding dopamine solution to it which is already discussed in the previous section and may be caused due to the refractive index of the solution. In Figure (2.13) the change is shown more clearly by comparing the signals separately for both the medium.

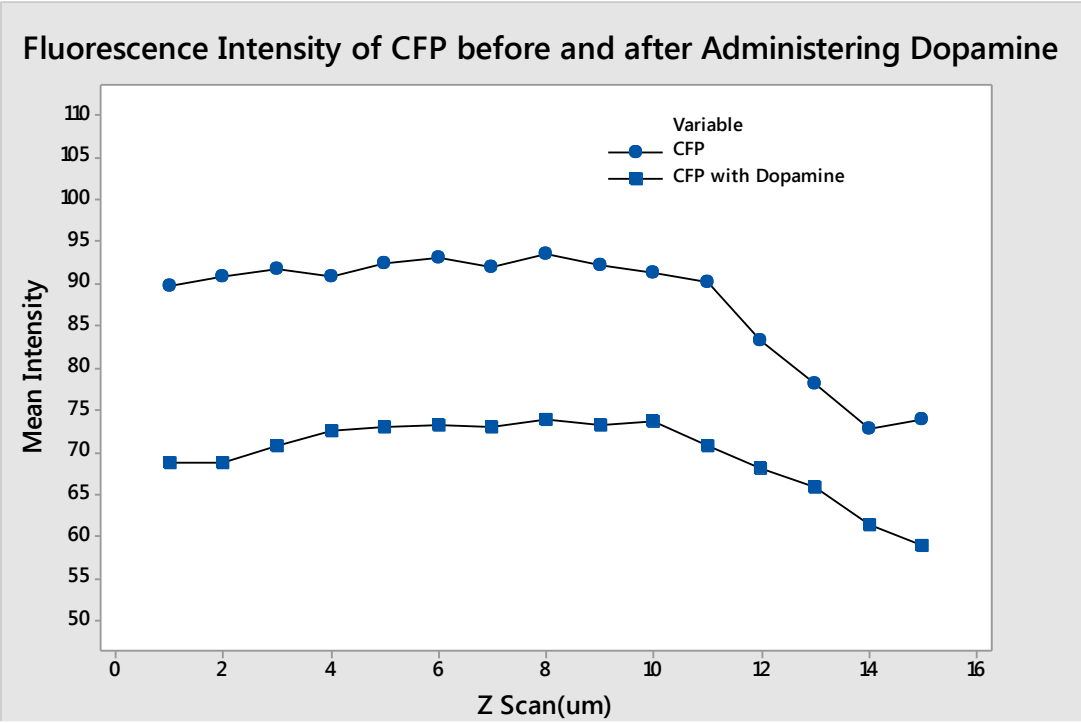

(a)

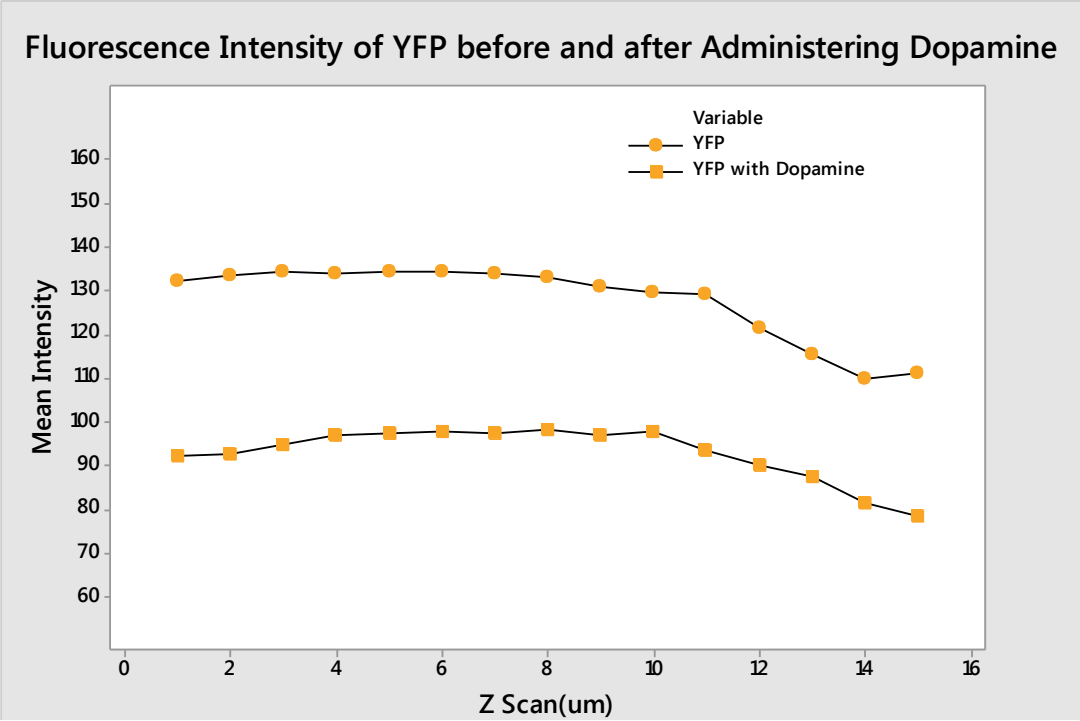

(b)

Figure 2.13 - (a) Fluorescence intensity of CFP before and after administering dopamine

(b) Fluorescence intensity of YFP before and after administering dopamine

Below in Figure (2.14 - a) shows the CFP and YFP fluorescence intensity ratio. The loss of ratio after adding dopamine solution to the sample exhibits the decrease in FRET due to the unfolding of EPAC1 by activation through cyclic AMP. This indicates the dopamine solution increases the amount of cyclic AMP which further shows the reducing number of activated exchange proteins. Figure (2.14 - b) depicts the percent change in ratio where the CFP/YFP ratio (R) was divided by the ratio (R_o) before administering dopamine. For statistical analysis $\Delta R/R_o$ is calculated for different Z-positions.

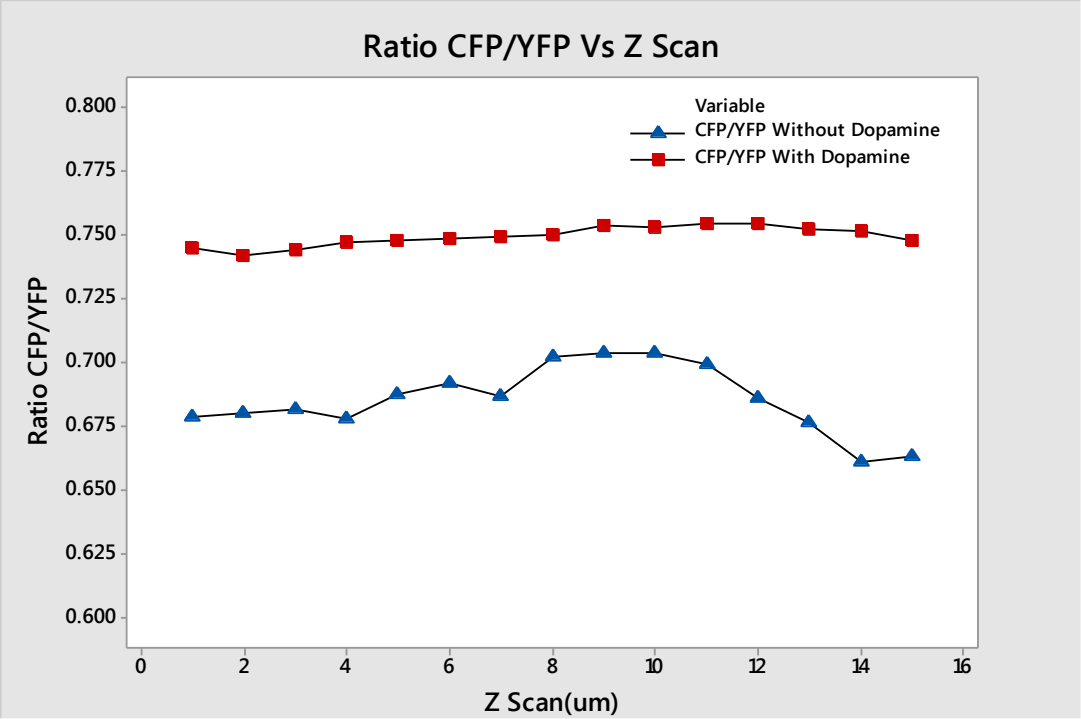
Ratio CFP/YFP Vs Z Scan
Variable
CFP/YFP Without Dopamine
CFP/YFP With Dopamine
Ratio CFP/YFP
0.800
0.775
0.750
0.725
0.700
0.675
0.650
0.625
0.600
0
2
4
6
8
10
12
14
16
Z Scan(um)

(a)

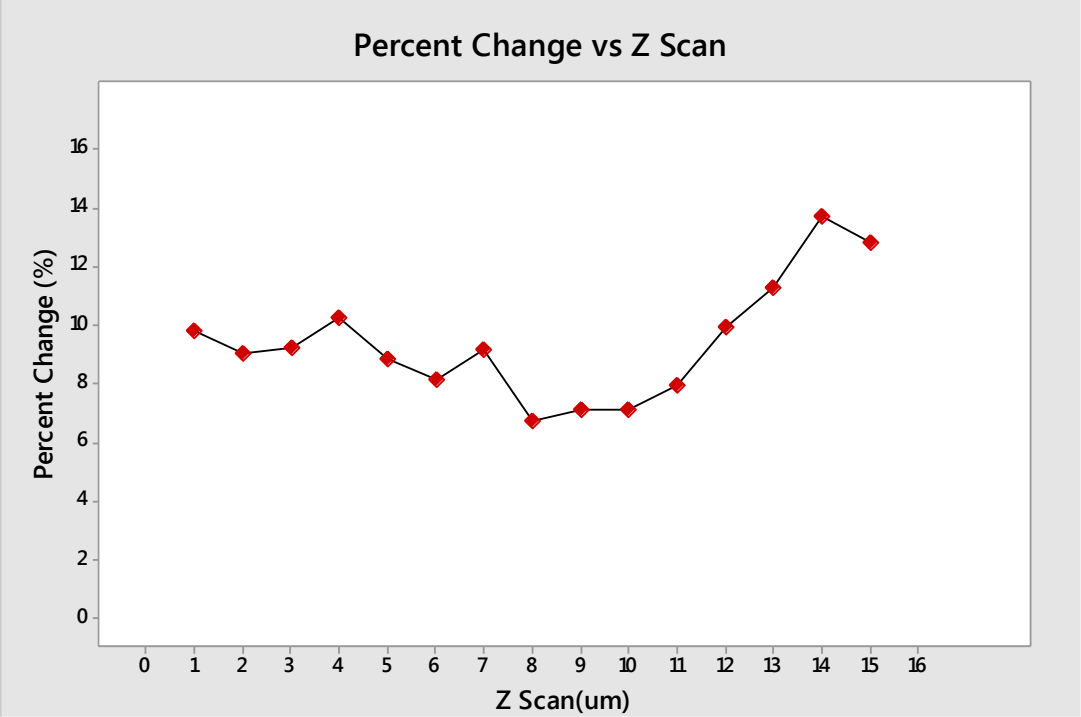
Percent Change vs Z Scan
Percent Change (%)
16
14
12
10
8
6
4
2
0
0
1
2
3
4
5
6
7
8
9
10
11
12
13
14
15
16
Z Scan(um)

(b)

Figure 2.14 - (a) Ratio of CFP and YFP fluorescence intensity before and after stimulating with dopamine

(b) Percent change in fluorescence intensity

2.9 CONCLUSION

The results has a positive indication of molecular structural change of the host protein (Epac1) due to protein-cAMP binding. The study shows that the CFP/YFP ratio inside a live *Drosophila melanogaster* mushroom bodies has increased after administering dopamine which suggests a decrease in Fluorescence Resonant Energy Transfer (FRET) between CFP-YFP pair. These are strong indication of dopaminergic modulation of cAMP production, which may be the reasons discussed for dopamine's role in the neural environments.

REFERENCES

1. Peter T. C. So, Chen Y. Dong, Barry R. Masters, and Keith M. Berland, Two-Photon Excitation Fluorescence Microscopy, Annu. Rev. Biomed. Eng. 2000. 02:399–429

2. Abbe, Ernst. "Ueber einen neuen Beleuchtungsapparat am Mikroskop." *Archiv für mikroskopische Anatomie* 9.1 (1873): 469-480.

3. G¨oppert-Mayer M. Uber elemen-tarakte mit zwei quantensprungen. *Ann. Phy 1931* 5:273–94.

4. Franken PA, Hill AE, Peters CW, Weinreich G. 1961. Generation of optical harmonics.Phys.Rev.Lett.7:118-19.

5. Kaiser W, Garrett CGB.1961.Two-phon excitation in CaF2:Eu2+.Phys.Rev.Lett. 7:229-31.

6. Singh S, Bradley LT. 1964. Three-photon absorption in naphthalene crystals by laser excitation.Phys.Rev.Lett.12:162-64.

7. Denk, Winfried, James H. Strickler, and Watt W. Webb. "Two-photon laser scanning fluorescence microscopy." *Science* 248.4951 (1990): 73-76.

8. Ruzin, Steve; Aaron, Holly. http://microscopy.berkeley.edu/courses/TLM/2P/index.html

9. Peter, T. C. "S. Two-photon fluorescence light microscopy. Encyclopedia of Life Science, 2002."

10. Theer, Patrick, Mazahir T. Hasan, and Winfried Denk. "Two-photon imaging to a depth of 1000 µm in living brains by use of a Ti: Al 2 O 3 regenerative amplifier." *Optics letters* 28.12 (2003): 1022-1024.

11. Peter, T. C. "S. Two-photon fluorescence light microscopy. Encyclopedia of Life Science, 2002."
12. Shafer, Orie T; et al. “Widespread Receptivity to Neuropeptide PDF throughout the Neuronal Circadian Clock Network of Drosophila Revealed by Real-Time Cyclic AMP Imaging”. Neuron 2008 58:223-237.
13. Kozlov, V. G., et al. "Laser action in organic semiconductor waveguide and double-heterostructure devices." *Nature* 389.6649 (1997): 362-364.
14. Förster, T. (1948). Intermolecular energy migration and fluorescence. Ann Physik (Leipzig) 2, 55–75.
15. Rahman, Nawreen, Jochen Buck, and Lonny R. Levin. "pH sensing via bicarbonate-regulated “soluble” adenylyl cyclase (sAC)." *Frontiers in physiology* 4 (2013).
16. Cheng, Xiaodong; Ji, Zhenyu; Tsalkova, Tamara; Mei, Fang. “Epac and PKA: a tale of two intracellular cAMP receptors”. Acta Biochem Biophys Sin (Shanghai) 2008 40(7):651-662.
17. "File:Cyclic-adenosine-monophosphate-2D-skeletal.png." *Wikimedia Commons, the free media repository*. 9 Feb 2015, 05:39 UTC. 30 Jun 2017, 07:12
18. File:Dopamine.svg." *Wikimedia Commons, the free media repository*. 12 Mar 2016, 07:23 UTC. 30 Jun 2017, 09:22
19. Greengard, Paul; Allen, Patrick B; Nairn, Angus C. “Beyond the Dopamine Receptor: the DARPP-32/Protein Phosphate-1 Cascade”. Neuron 1999 23:435-447.
20. Bäckman, Lars; Lindenberger, Ulman; Li, Shu-Chen; Nyberg, Lars. “Linking cognitive aging to alterations in dopamine neurotransmitter functioning: Recent data and future avenues”. Neuroscience and Biobehavioral Reviews 2010 34:670-677.

21. Periasamy, Ammasi. "Fluorescence resonance energy transfer microscopy: a mini review." *Journal of biomedical optics* 6.3 (2001): 287-291.

22. Thaler, Christopher; Vogel, Steven S. “Quantitative Linear Unmixing of CFP and YFP from Spectral Images Acquired with Two-Photon Excitation”. Cytometry Part A 2006 69A:904-911.

23. De Rooij, Johan, et al. "Epac is a Rap1 guanine-nucleotide-exchange factor directly activated by cyclic AMP." *Nature* 396.6710 (1998): 474-477.

24. Kawasaki, Hiroaki, et al. "A family of cAMP-binding proteins that directly activate Rap1." *Science* 282.5397 (1998): 2275-2279.

25. Weber, Irene T., et al. "Predicted structures of cAMP binding domains of type I and II regulatory subunits of cAMP-dependent protein kinase." *Biochemistry* 26.2 (1987): 343-351.

26. Boto, Tamara, et al. "Dopaminergic modulation of cAMP drives nonlinear plasticity across the Drosophila mushroom body lobes." *Current Biology* 24.8 (2014): 822-831.

27. Eric, C. R. "Drosophila melanogaster: The fruit fly. Encyclopedia of genetics." (2001).

28. October 16, 2007, at the Wayback Machine. at lsbu.ac.uk Water Structure and Science.

VITA

Syeed Ehsan Ahmed was born and raised in Dhaka, Bangladesh. He earned his bachelor degree in Physics from University of Dhaka, Bangladesh in 2013. He joined the University of Texas at El Paso (UTEP) in fall 2015 as a Master's student in the Physics Department. During his Master's studies, he worked as a teaching assistant at UTEP in Physics Department. Since fall 2015 Syeed has worked in the field of nonlinear optical microscopy and spectroscopy with applications in biophysics with Dr. Chunqiang Li in his Biophotonics laboratory. He plans to continue his education at Washington State University in pursuit of a Ph.D. in Physics where he will continue research in the area of nonlinear optics and biophysics.